

Unified Domain Adaptive Semantic Segmentation

Zhe Zhang^{id}, Gaochang Wu^{id}, Jing Zhang^{id}, Xiatian Zhu^{id}, Dacheng Tao^{id}, *Fellow, IEEE*,
Tianyou Chai^{id}, *Life Fellow, IEEE*

Abstract—Unsupervised Domain Adaptive Semantic Segmentation (UDA-SS) aims to transfer the supervision from a labeled source domain to an unlabeled target domain. The majority of existing UDA-SS works typically consider images whilst recent attempts have extended further to tackle videos by modeling the temporal dimension. Although the two lines of research share the major challenges – overcoming the underlying domain distribution shift, their studies are largely independent. This causes several issues: (1) The insights gained from each line of research remain fragmented, leading to a lack of a holistic understanding of the problem and potential solutions. (2) Preventing the unification of methods, techniques, and best practices across the two domains, resulting in redundant efforts and missed opportunities for cross-pollination of ideas. (3) Without a unified approach, the knowledge and advancements made in one domain (images or videos) may not be effectively transferred to the other, leading to suboptimal performance and slower progress. Under this observation, we advocate unifying the study of UDA-SS across video and image scenarios, enabling a more comprehensive understanding, synergistic advancements, and efficient knowledge sharing. To that end, we explore the unified UDA-SS from a general data augmentation perspective, serving as a unifying conceptual framework, enabling improved generalization, and potential for cross-pollination of ideas, ultimately contributing to the overall progress and practical impact of this field of research. Specifically, we propose a Quad-directional Mixup (QuadMix) method, characterized by tackling distinct point attributes and feature inconsistencies through four-directional paths for intra- and inter-domain mixing in a feature space. To deal with temporal shifts with videos, we incorporate optical flow-guided feature aggregation across spatial and temporal dimensions for fine-grained domain alignment. Extensive experiments show that our method outperforms the state-of-the-art works by large margins on four challenging UDA-SS benchmarks. Our source code and models will be released at <https://github.com/ZHE-SAPI/UDASS>.

Index Terms—Unified domain adaptation, semantic segmentation, QuadMix, flow-guided spatio-temporal aggregation.

I. INTRODUCTION

SEMANTIC segmentation attempts to make precise dense predictions relevant to assigning a unique label to every single pixel within images or video frames, vital for a broad range of critical applications, such as autonomous driving [1], [2], medical imaging [3], [4], and so forth. However, when adapting to unseen and unlabeled video or image domains,

the model performance always drops largely due to significant domain gaps at spatial [5] or temporal [6] levels, which limits their usability and deployability. Moreover, manual pixel-level annotation is labor-intensive [7], while labels of synthetic data rendered by game engines [8]–[10] are freely available. This has led to growing interest in Unsupervised Domain Adaptive Semantic Segmentation (UDA-SS), which transfers knowledge from a labeled source domain (synthetic) to an unlabeled target domain (real). However, despite the shared challenges in video (UDA-VSS) and image (UDA-ISS) scenarios, research in these areas is largely independent, leading to a lack of holistic understanding of the problem and potential solutions.

At present, there is not so substantial research on UDA-VSS. The community pays more attention to UDA on image scenarios, plenty of works [5], [11]–[23] address syn2real adaptation by joint learning. The methods for UDA-ISS can be roughly divided into two lines. The first line is based on domain alignment to reduce feature distribution discrepancies explicitly or implicitly. In practice, intermediate domain bridging [19], [21]–[24], adversarial training [25]–[27], and statistical measure minimizing [28]–[30] have been proposed to diminish the domain gap. Despite the fact that they can pull the target domain distribution to the source domain, it does not guarantee the domain gap within each category-aware feature space can be solved, because pixels across domains could share similar semantics but feature quite distinct visual characteristics. Another line is self-supervised learning, adopting confidence filtering [5], [31], label denoising [32], [33] or regularization [14], [34]. However, obtaining pseudo-labels is not easy when large gaps exist between distinct domains and always only denoised or high-confidence labeled samples are involved in self-supervised learning.

Naturally, existing UDA-ISS methods are not directly suitable for videos, owing to domain gaps not just at spatial but also temporal levels [35], and the object motion is complex [36]. Recently, several UDA-VSS methods based on self-supervised video learning or domain alignment strategies have been proposed [36]–[38]. In practice, they employ fine-designed auxiliary clues involving optical flow or geometric motion to constrain pixel-class consistency among adjacent frames. Moreover, techniques like one-way mixed intermediate video domain [39] stage-wisely or adversarial training [6], [35] have emerged to align feature distribution across domains. Nevertheless, similar to UDA-ISS works, the persistent domain gap in spatio-temporal feature embeddings hindered the knowledge transfer and reliable pseudo-label generation.

However, fragmented insights from independent scenarios often lead to redundant efforts and missed opportunities for cross-pollination, resulting in slower progress and suboptimal

Zhe Zhang, Gaochang Wu, and Tianyou Chai are with the State Key Laboratory of Synthetical Automation for Process Industries, Northeastern University, Shenyang, China. Email: zhangzhe17@stumail.neu.edu.cn, wugc@mail.neu.edu.cn, tychai@mail.neu.edu.cn.

Xiatian Zhu is with the Surrey Institute for People-Centred Artificial Intelligence, and Centre for Vision, Speech and Signal Processing, University of Surrey, Guildford, UK. E-mail: xiatian.zhu@surrey.ac.uk.

Jing Zhang and Dacheng Tao are with the School of Computer Science, Faculty of Engineering, University of Sydney, Sydney, Australia. E-mail: jing.zhang1@sydney.edu.au and dacheng.tao@sydney.edu.au.

Corresponding author: Tianyou Chai.

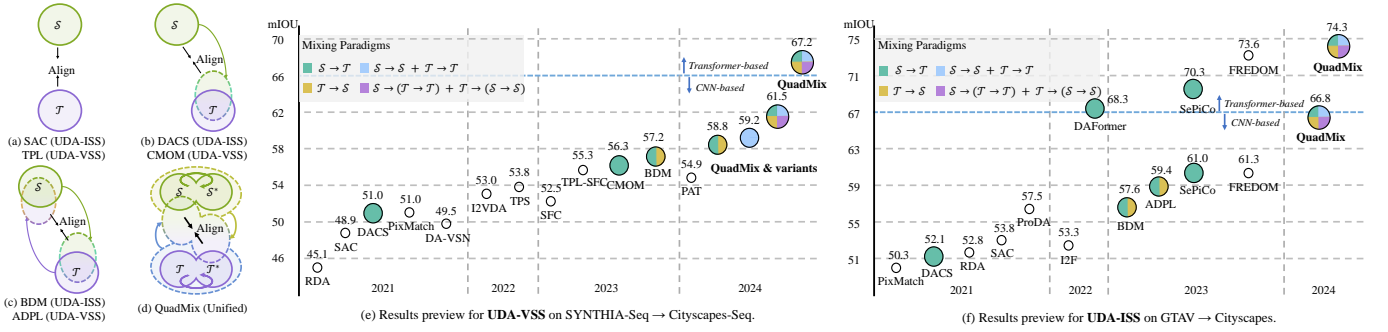


Fig. 1. Source domain: \mathcal{S} , target domain: \mathcal{T} . Unlike existing methods that address UDA-SS for videos or images separately, we offer a unified solution to tackle the shared major challenge of insufficient feature gap bridging caused by **distinct point attributes**. (a)–(d): Mixing paradigms comparison. Our unified QuadMix method comprehensively bridges the image/video gap at both spatial (temporal) pixel- and feature-levels. Specifically, we adaptively generate enhanced **inter-mixed** domains deriving from generalized **intra-mixed** domains. (e)–(f): Preview of result examples for the UDA-VSS and UDA-ISS.

performance. From a unified view, current state-of-the-art methods achieve impressive results by addressing domain gaps through meticulously designed intermediates for image [19], [21]–[24] and video [39] scenarios. However, we find that the compact nature of features within each domain (**intra-domain**) causes source and target domains to be represented as two **distinct points** [40], resulting in the intermediates with poorly generalized distributions for hard gap bridging. As shown in Fig. 1(a)–(d), we present a comparison of existing methods, distinguishing source features in green and target features in purple. Inspired by [41], [42], strategies like one-way mixing (e.g., [19], [23], [24], [39]) or two-way mixing (e.g., [21], [22]) extensively explore the integration of source pixel-level patches into the target domain, or vice versa, aiming to bridge the domain gap explicitly. Nonetheless, as supported by the t-SNE analysis [43] in Fig. 7(a)(c)(d), the effect of existing one-/two-way mixed intermediates across domains (**inter-domain**) that derived from such distinct domains is fragmentary and insufficient, which continues to hinder knowledge transfer to the target domain. Moreover, pure pixel-level mixing may lead to model confusion because of **feature inconsistencies** caused by distinct domain contexts.

In this paper, we explore UDA-SS for video and image scenarios within a unified framework to promote cross-pollination of ideas. As shown in Fig. 1(d), we propose a Quad-directional Mixup (QuadMix) method to address the above challenge for comprehensive domain gap bridging. To tackle complex video temporal feature shifts, we further propose a flow-guided spatio-temporal feature aggregation module for domain alignment, which can also be extended to images.

Firstly, QuadMix comprises comprehensive mixing paths in four directions designed for intra- and inter-domains. Unlike existing methods that struggle with insufficient inter-domain mixing caused by distinct point attributes, we smooth features within each domain to create more generalized **intra-mixed** domains, which are then merged to generate more enhanced **inter-mixed** domains. Technically, we generate adaptive category-aware video/image patch templates from two domains on the fly, which are then internally fused with their original domains to create intra-mixed source ($\mathcal{S} \rightarrow \mathcal{S}$) and target ($\mathcal{T} \rightarrow \mathcal{T}$) domains with generalized feature embeddings. Additionally, both pixel level and feature level patch tem-

plates are interactively fused with the intra-mixed domains to construct more enhanced inter-mixed source ($\mathcal{T} \rightarrow (\mathcal{S} \rightarrow \mathcal{S})$) and target ($\mathcal{S} \rightarrow (\mathcal{T} \rightarrow \mathcal{T})$) domains, as depicted in Fig. 7(e). Critically, we conduct the QuadMix at both spatial (temporal) pixel and feature levels to alleviate **feature inconsistencies** arising from diverse domain-wise contexts across quad-mixed domains. Consequently, it bridges domain gaps sufficiently within an enhanced feature embedding space, facilitating effective knowledge transfer from source to target domain.

Furthermore, for UDA-VSS, to better mitigate spatial and temporal gaps for enhanced pixel-level discrimination, we propose an adaptive spatio-temporal feature aggregation module guided by optical flow for domain alignment, which can also be extended to UDA-ISS. Typically, inherent feature gaps across source and target domains often lead to scattered distributions within each category and overlapping across categories, posing challenges to domain adaptation. To address this, we propose optical flow-guided spatial aggregation for precise fine-grained feature extraction, integrating temporal clues into spatial features to maintain temporal consistency. Following this, we conduct entropy-based temporal aggregation across consecutive frames to enhance overall temporal coherence. This module effectively utilizes temporal clues to extract and aggregate video features across domains, enabling fine-grained feature alignment for enhanced adaptation.

In a nutshell, our contributions can be summarized:

- Through addressing the shared major challenge of underlying domain distribution shift, *for the first time*, we study UDA-SS for video and image from a unified view by comprehensive quad-mixing at pixel and feature levels.
- To further tackle the complex spatio-temporal shift within videos, we propose a flow-guided spatio-temporal feature aggregation module for fine-grained alignment, which can also be extended to image scenarios.
- Extensive experiments on four popular benchmarks show that we achieve superior results in unified scenarios. Particularly, we obtain mIoUs of 61.5%, 56.2%, 66.8%, and 62.6% on Synthia-Seq \rightarrow Cityscapes-Seq, VIPER \rightarrow Cityscapes-Seq, GTAV \rightarrow Cityscapes, and Synthia \rightarrow Cityscapes, respectively. The former two are UDA-VSS benchmarks and the latter two are UDA-ISS benchmarks. Equipped with Transformer, we further improve mIoUs

by 5.7%, 2.0%, 9.3%, and 4.9%, respectively, setting the new state-of-the-arts. Ablation studies and detailed analysis verify the effectiveness.

II. RELATED WORK

A. Unsupervised Domain Adaption for Image Segmentation

UDA-ISS has garnered significant attention in both theoretical and practical research. At the image level, the mainstream is to transfer image styles while preserving original semantics. Various approaches including cycle translation [25], patch adversarial [44], dual path learning [22], and text-to-image diffusion models [45] have been proposed. At the feature level, influential metrics and their variants [29], [30], [46] are developed to address distribution discrepancies across domains. Additionally, using prototypes to represent feature centroids has been crucial in pseudo-label denoising [47], divergence measurement [32], [48], and contrastive learning [23], [49]. At the output level, adversarial adaptation on low-dimensional logit space has been proposed in [50]. Other works, such as progressive confidence [51] and curriculum learning [52], [53], aim to refine target pseudo-labels within a structured output space [54]. Moreover, from the perspective of feature distribution, generating intermediate domains via one-way [19], [23], [24] or two-way pixel-level mixing [21], [22] to bridge feature gaps has yielded impressive results. However, *distinct point attributes* and *feature inconsistencies* are major challenges that often hinder effective knowledge transfer, which also exist in video scenarios. While UDA-ISS has been widely studied, UDA-VSS is still in its early stages. In this paper, we are the first to **unify the study** of these two tasks to address the shared major challenges. Notably, previous methods handle cross-domain features separately without interaction [19], [21]–[24], whereas we enhance this by performing QuadMix at the feature level to alleviate feature inconsistencies.

B. Video Semantic Segmentation

Video Semantic Segmentation (VSS) involves pixel-level classification for consecutive frames and has gained increasing attention powered by deep neural networks and densely labeled datasets [55], [56]. Mainstream works focus on leveraging temporal relationships to enhance segmentation accuracy. Techniques such as motion-guided feature warping [57] and prediction warping [58], along with temporal propagation via recurrent networks [59] or auxiliary networks [60], have been developed. Sun et al. [61] further propose a coarse-to-fine method to capture static and dynamic contextual features. To improve inference efficiency, Hu et al. [62] suggest using weight-sharing subnetworks across frames and reconstructing spatial features through attention mechanisms [63]. Recently, semi- and weakly-supervised VSS have gained increasing attention. Lao et al. [64] introduce a feature enhancement network that models both short-term and long-term temporal dependencies, while IFR [65] presents a feature reconstruction technique to reduce inner-video overfitting and utilizes partial labels to guide the learning of unlabeled frames.

However, existing VSS works heavily rely on dense labels, making it difficult to adapt to shifted and unlabeled target

videos. In this paper, we study domain adaptation to address this issue. Notably, we leverage **video temporal clues** by (1) using optical flow to generate cross-frame consistent target pseudo-labels; (2) integrating temporal clues into spatial features for each domain; and (3) aggregating spatial features across consecutive frames for fine-grained domain alignment.

C. Unsupervised Domain Adaptive Video Segmentation

Research on video domain adaptation initially emerged for action recognition, emphasizing sparse classification of entire video clips [66]–[69]. Recently, interest in UDA-VSS has surged due to the rising demand for dense video perception. Pioneering works [6], [35] employ adversarial learning with DCGAN [70] to extract domain-invariant video features. Guan et al. [6] further refine this by aligning uncertain target predictions with more confident adjacent ones. However, asynchronous issues with generator-discriminator convergence often cause training instability. Additionally, auxiliary clues involving geometric motion [36] or optical flow [37], [38] are introduced to generate pseudo-labels for self-supervised learning. However, they train the model on samples from each domain alternately but overlook domain interactions, leading to isolated learning that hampers adaptation to the target domain. Meanwhile, Wu et al. [71] explore transferring spatial knowledge from image to video domains while overlooking temporal feature gaps. Cho et al. [39] perform one-way input-level mixing from source to target but fail to address distinct point attributes across domains. In addition, they only align single-frame spatial features, heavily relying on a pre-trained model from [6] to generate initial pseudo-labels and initialize model parameters. In contrast, our method is trained end-to-end and further mitigates temporal shifts.

Based on the above analysis, we propose a unified method to tackle intra-domain *distinct point attributes* that hinder effective video/image domain gap bridging. For video scenarios, we further utilize temporal clues and propose flow-guided feature aggregation for fine-grained domain alignment. We are the first to explore UDA-VSS using **advanced transformer networks**.

III. METHOD

A. Method Overview

UDA-SS transfers segmentation knowledge from a labeled source domain to a related but shifted target domain without pixel-level labels. In this paper, we unify the study of video and image scenarios to address shared challenges posed by the large feature gap, promoting a deeper understanding and efficient knowledge sharing. Naturally, the inputs differ between the two scenarios. For UDA-VSS, let $X_t^S = \mathbb{S}\{x_{t-1}^S, x_t^S\}$ with $o_{t-1 \rightarrow t}^S$ representing source adjacent frames alongside optical flow, and y_t^S to be truth label of x_t^S , where \mathbb{S} denotes a stack operation along time dimension. The target frames and optical flow are $X_t^T = \mathbb{S}\{x_{t-1}^T, x_t^T\}$ with $o_{t-1 \rightarrow t}^T$ but without label y_t^T . For UDA-ISS, the source image and label are denoted as x^S and y^S while the target image is x^T without label y^T . The goal is to overcome the large domain gap and develop a model that effectively generalizes to the target domain.

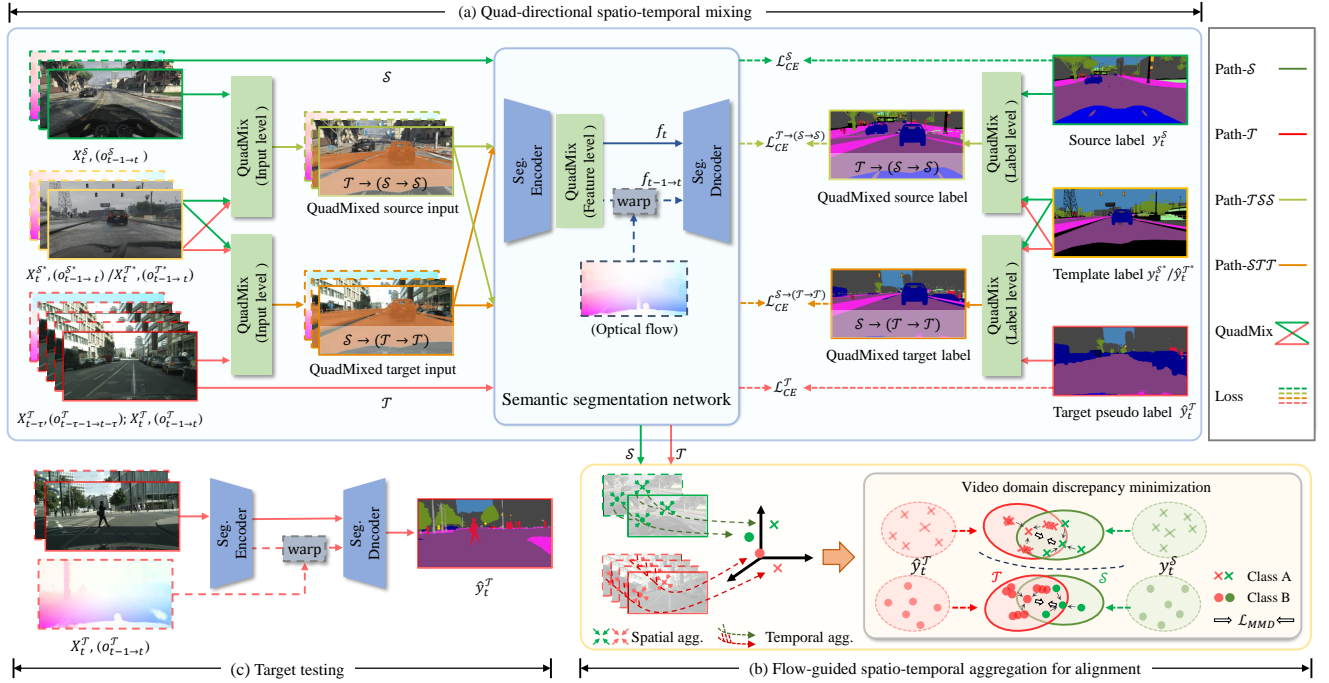


Fig. 2. Overview of the proposed QuadMix for UDA-SS. *UDA-ISS* follows a parallel approach, with the exception of temporal clues, as indicated by the dashed lines. The model is jointly trained using labeled source videos and unlabeled target videos. (i) In part (a), QuadMix comprises four comprehensive intra/inter-domain mixing paths to bridge domain gaps at spatio-temporal pixel and feature levels. Pixel-level mixing is performed on adjacent frames, optical flow, and labels/pseudo-labels, aiming to generate two enhanced inter-mixed domains derived from intra-mixed domains iteratively: $\mathcal{T} \rightarrow (\mathcal{S} \rightarrow \mathcal{S})$ and $\mathcal{S} \rightarrow (\mathcal{T} \rightarrow \mathcal{T})$. These intermediates overcome *distinct point attributes* within \mathcal{S} and \mathcal{T} , exhibiting more enhanced features for gap bridging. Additionally, feature-level mixing across quad-mixed domains alleviates *feature inconsistencies* caused by distinct domain-wise video contexts; (ii) In part (b), optical flow-guided spatio-temporal aggregation compresses video features across domains into a compacted category-aware space, minimizing intra-category discrepancies and enhancing inter-category discriminability for target domain; (iii) The training process is end-to-end. In part (c), stacked adjacent frames X_t^T and optical flow O_{t-1-t}^T are needed for target domain testing.

In this paper, we propose a unified method named QuadMix to bridge and mitigate the significant video or image domain gap within an explicit feature space. As depicted in Fig. 2, to address the shared major challenge of *fragmentary and insufficient gap bridging*, QuadMix integrates four-directional paths designed for both intra- and inter-domains, operating at both input, feature, and label levels. Furthermore, we propose the adaptive spatio-temporal feature aggregation guided by optical flow for fine-grained domain alignment, which can also extend to image scenarios. To generate accurate pseudo-labels \hat{y}_t^T for self-supervised learning, for UDA-VSS, we input $X_{t-\tau}^T = \mathbb{S}\{x_{t-\tau-1}^T, x_{t-\tau}^T\}$ and $O_{t-\tau-1 \rightarrow t-\tau}^T$ from previous timestamp into the model to obtain $\hat{y}_{t-\tau}^T$, which is then warped using $O_{t-\tau \rightarrow t}^T$ to generate temporally coherent \hat{y}_t^T , where τ denotes video temporal deviation. For UDA-ISS, the pseudo-labels are generated by a momentum network [72].

As analyzed earlier, current methods always struggle with distinct point attributes which result in insufficient bridging, whilst purely pixel-level mixing often leads to feature inconsistencies. To address this, as illustrated in Fig. 2(a), our QuadMix first adaptively generates category-aware video patch templates online from two domains (marked in yellow or blue). These templates are utilized to create two intra-mixed domains with smoother and generalized feature embeddings, addressing the feature compactness within each domain. Building on this, we perform interactive mixing to generate two more enhanced inter-mixed domains, serving as comprehensive intermediates

for gap bridging. QuadMix not only involves spatial (frames and labels) and temporal (optical flow), but also spatio-temporal feature-level mixing. For UDA-ISS, QuadMix is similar while excluding temporal clues.

Besides the spatial feature gap common to both scenarios, video data also faces a temporal gap. For UDA-VSS, we propose an adaptive flow-guided spatial-temporal feature aggregation module for fine-grained domain alignment (Fig. 2(b)). Spatial-level aggregation is guided by source/target pseudo masks adaptively online, while at the temporal level, features are further integrated based on logit entropy to enhance overall temporal coherence. Notably, each frame’s spatial feature is enriched with information from previous frames via optical flow propagation. Based on this, the aggregated features across domains are fine-grained aligned, thereby improving pixel-level discrimination for the target domain. This module can also be extended to UDA-ISS using spatial aggregation.

B. Video/Image Patch Templates Generation Across Domains

The domain gap becomes more evident when we observe diverse objects’ motion at the category-aware level. To mitigate the *distinct point attributes* across two domains existing in both video and image scenarios, we propose bridging and generalizing features by intra- and inter-domain mixing quad-directionally. This design necessitates the adaptive generation of reliable and diverse video/image patch sequences as templates, as denoted in Fig. 3. In this paper, we adaptively

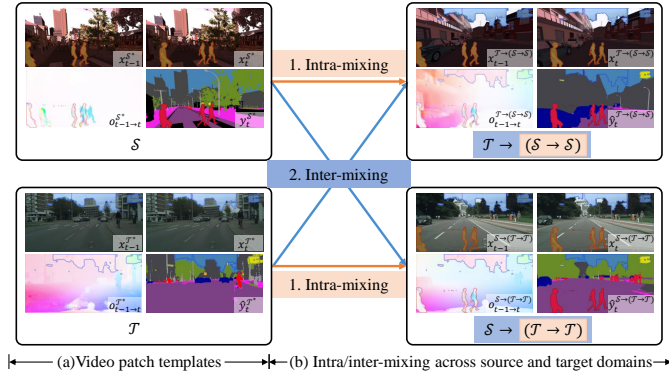


Fig. 3. Example illustration of video patch templates (see Eq. (1)) and intra-/inter-mixing for **UDA-VSS**. In part (a), video patch templates involve category-aware pixel regions (e.g., *person* and *rider* of \mathcal{S} (highlighted by yellow masks), *sign* and *sky* of \mathcal{T} (highlighted by blue masks)) of video frames, optical-flow, and labels/pseudo-labels. In part (b), we start with intra-domain mixing and subsequently proceed to inter-domain mixing. The generated quad-mixed domains serve as comprehensive intermediates to bridge domain gaps. Notably, video patch templates required in training iteration n are generated online adaptively from iteration $n - 1$. Please zoom in for details.

generate cross-domain patch templates online. Specifically, for training iteration n , the source domain patch templates $Z_{t,n}^{\mathcal{S},k}$, $k \in K_{\mathcal{S}}$ and target domain patch templates $Z_{t,n}^{\mathcal{T},k}$, $k \in K_{\mathcal{T}}$ required for quad-directional mixing are derived from the previous iteration $n - 1$, where symbol “*” denotes templates. These patch templates contain pixel regions belonging to specific categories k , which are randomly selected from segmentation label spaces $K_{\mathcal{S}}$ and $K_{\mathcal{T}}$, respectively.

For **UDA-VSS**, video patch templates form a unified set of category-aware adjacent frames, labels/pseudo-labels, and optical flow. The target video patch template is defined as:

$$Z_{t,n}^{\mathcal{T},k} = \left\{ X_{t,n-1}^{\mathcal{T},k}, \hat{y}_{t,n-1}^{\mathcal{T},k}, o_{t-1 \rightarrow t,n-1}^{\mathcal{T},k} \right\}, \quad (1)$$

specifically,

$$X_{t,n-1}^{\mathcal{T},k} = X_{t,n-1}^{\mathcal{T}} \odot \mathbb{1}(\mathcal{F}(\hat{Y}_{t,n-1}^{\mathcal{T}}) == k), \quad (2)$$

$$\hat{y}_{t,n-1}^{\mathcal{T},k} = \hat{y}_{t,n-1}^{\mathcal{T}} \odot \mathbb{1}(\mathcal{F}(\hat{y}_{t,n-1}^{\mathcal{T}}) == k), \quad (3)$$

$$o_{t-1 \rightarrow t,n-1}^{\mathcal{T},k} = o_{t-1 \rightarrow t,n-1}^{\mathcal{T}} \odot \mathbb{1}(\mathcal{F}(\hat{y}_{t-1,n-1}^{\mathcal{T}}) == k), \quad (4)$$

where $k \in K_{\mathcal{T}^*}$ and corresponding to two selected categories, $\mathbb{1}(\cdot)$ is the indicator function, \odot refers to a pixel mapping operation by position-wise multiplication, and \mathcal{F} stands for a target filtering operation based on the confidence level of segmentation logits. Detailed depictions are shown in Fig. 4(a)(c).

Notably, the model takes $X_t = \mathbb{S}\{x_{t-1}, x_t\}$ with $o_{t-1 \rightarrow t}$ (indices omitted) as inputs and generates a segmentation map for x_t . Therefore, the bottom-right time subscripts of pseudo-labels are t in Eq. (3) and $t - 1$ in Eq. (4) for corresponding category-aware masks. Additionally, $\hat{Y}_t^{\mathcal{T}} = \mathbb{S}\{\hat{y}_{t-1}^{\mathcal{T}}, \hat{y}_t^{\mathcal{T}}\}$, the generation of which will be shown in Eq. (17). In this paper, masks for pixel mapping evolve with pseudo labels rather than being pre-generated offline as in [21], [39], avoiding the accuracy limitation imposed by a frozen warm-up model.

The source video patch template $Z_{t,n}^{\mathcal{S},k}$, $k \in K_{\mathcal{S}}$ follows a pattern parallel to Eq. (1), just needing to replace \mathcal{T} with

\mathcal{S} and employ source labels instead of target pseudo-labels in Eq. (1) to Eq. (4). To promote feature diversity within quad-mixed domains, we ensure that the categories k of video patch templates differ across domains at each training iteration.

For **UDA-ISS**, the image patch template also forms a set but excludes temporal clues as in the video domain, which is denoted as $Z_{t,n}^{\mathcal{T},k} = \left\{ x_{t,n-1}^{\mathcal{T},k}, \hat{y}_{t,n-1}^{\mathcal{T},k} \right\}$ for the target domain, and $Z_{t,n}^{\mathcal{S},k}$ similarly for the source domain.

In this way, we generate category-aware patch templates online as templates, which are then utilized for quad-directional mixing to bridge domain gaps in video or image scenarios.

C. Intra-Mixed Video/Image Domain Adaptation

According to Fig. 1(a) and feature visualization in Fig. 7(a), despite the semantic similarity between source and target domains, a notable feature gap often persists in spatial structure and temporal coherence. Fig. 3(b) presents a depiction of four mixed paths of QuadMix. Rather than purely alternative training with cross-domain data [5], [37], or one way [19], [23], [24], [39]/bidirectional [21], [22] data pasting guided by offline-generated pseudo-labels via warm-up models stage-wisely, we propose a comprehensive QuadMix trained end-to-end. A more detailed process is shown in Fig. 4. In this section, we present the intra-mixed domain adaptation.

1) *Target to Target Mixing ($\mathcal{T} \rightarrow \mathcal{T}$)*: From the view of feature distribution, we consider source and target video/image domains as two distinct points featured with discontinuous and compact intra-domain feature distribution, and significant inter-domain feature gap. In this section, to address *distinct point attributes* within each domain for better gap bridging, we propose smoothing and generalizing intra-domains within an explicit feature space for the target domain.

For **UDA-VSS**, adaptive target video patch templates are iteratively integrated into target domain samples, guided by pseudo mask sequences. The process unfolds as follows:

$$X_{t,n}^{\mathcal{T} \rightarrow \mathcal{T}} = X_{t,n-1}^{\mathcal{T},k} + X_{t,n}^{\mathcal{T}} \odot (1 - M_{t,n-1}^{\mathcal{T},k}), \quad (5)$$

$$\hat{y}_{t,n}^{\mathcal{T} \rightarrow \mathcal{T}} = \hat{y}_{t,n-1}^{\mathcal{T},k} + \hat{y}_{t,n}^{\mathcal{T}} \odot (1 - m_{t,n-1}^{\mathcal{T},k}), \quad (6)$$

$$o_{t-1 \rightarrow t,n}^{\mathcal{T} \rightarrow \mathcal{T}} = o_{t-1 \rightarrow t,n-1}^{\mathcal{T},k} + o_{t-1 \rightarrow t,n}^{\mathcal{T}} \odot (1 - m_{t-1,n-1}^{\mathcal{T},k}), \quad (7)$$

for simplicity, Eq. (5) to Eq. (7) can be simplified as follows:

$$Z_{t,n}^{\mathcal{T} \rightarrow \mathcal{T}} = Z_{t,n}^{\mathcal{T},k} + Z_{t,n}^{\mathcal{T}} \odot (1 - M_{t,n-1}^{\mathcal{T},k}), \quad (8)$$

where $M_{t,n-1}^{\mathcal{T},k} = \mathbb{S}\{m_{t-1,n-1}^{\mathcal{T},k}, m_{t,n-1}^{\mathcal{T},k}\}$ is the category-aware binary pseudo mask sequence corresponding to video patch template $Z_{t,n}^{\mathcal{T},k}$, $k \in K_{\mathcal{T}}$, with a resolution of $B \times H \times W$, where B is the batch size. It can be denoted as follows:

$$M_{t,n-1}^{\mathcal{T},k} = \mathbb{1}(\mathcal{F}(\hat{Y}_{t,n-1}^{\mathcal{T}}) == k), k \in K_{\mathcal{T}}, \quad (9)$$

in this way, we iteratively integrate category-aware target video templates alongside target video samples mapped by $1 - M$ to generate data for the intra-mixed target domain.

For **UDA-ISS**, the generated target to target mixing samples $Z_{t,n}^{\mathcal{T} \rightarrow \mathcal{T}}$ can be performed following Eq. (8) using $M_{t,n-1}^{\mathcal{T},k} = m_{t,n-1}^{\mathcal{T},k}$, without the optical flow-level mixing as in Eq. (7).

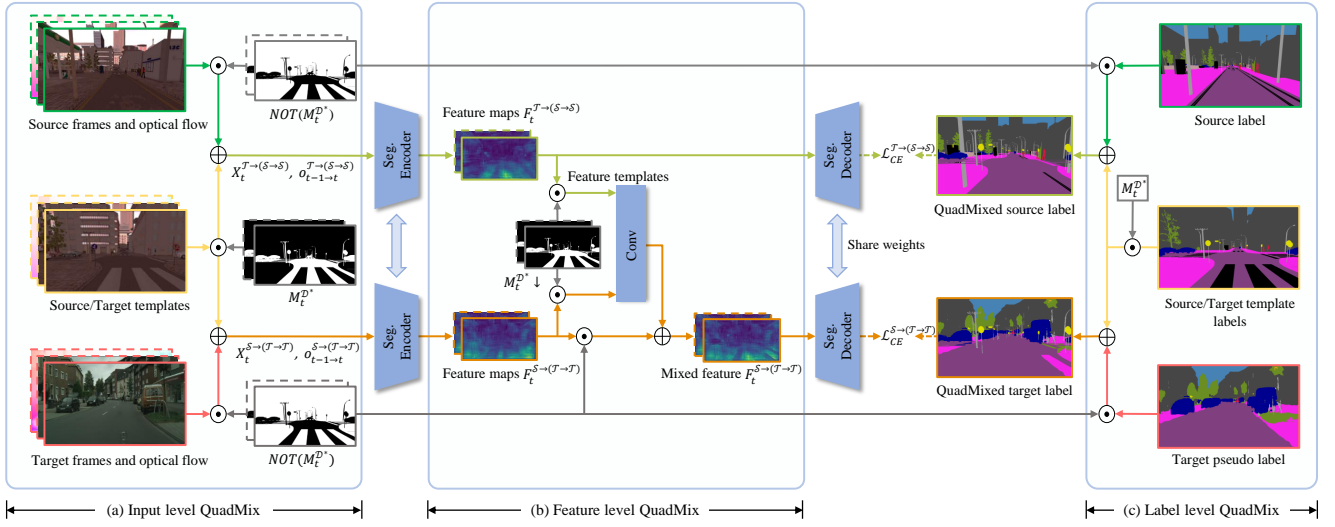


Fig. 4. Detailed illustration of the quad-directional mixing for UDA-SS. To alleviate distinct point attributes for comprehensive domain gap bridging, we conduct QuadMix at the spatial level (video adjacent frames and label), temporal level (optical flow), and spatio-temporal feature level, constructing more enhanced inter-mixed source ($\mathcal{T} \rightarrow (\mathcal{S} \rightarrow \mathcal{S})$) and inter-mixed target ($\mathcal{S} \rightarrow (\mathcal{T} \rightarrow \mathcal{T})$) domains that derived from intra-mixed domains ($\mathcal{S} \rightarrow \mathcal{S}$) and ($\mathcal{T} \rightarrow \mathcal{T}$) with concentrated feature spaces. The mask M_t^{D*} denotes the union of source patch template mask M_t^{S*} and target patch template mask M_t^{T*} .

Generally, spatial-level intra-domain mixing is detailed in Eq. (5) and Eq. (6), while temporal-level mixing is specified in Eq. (7), where n denotes the training iteration, and t represents the timestamp of adjacent frames within each iteration.

2) *Source to Source Mixing ($\mathcal{S} \rightarrow \mathcal{S}$)*: As illustrated in Fig. 3(b), the generation of the intra-mixed source domain follows a similar pattern to that of the target domain. To achieve this, we substitute \mathcal{T} with \mathcal{S} in Eq. (8) and replace $\mathcal{F}(\hat{Y}_{t,n-1}^{\mathcal{T}*})$ with the source domain labels $Y_{t,n-1}^{\mathcal{S}*}$ in Eq. (9), which leverage rich semantic segmentation annotations available in the source domain. It can be denoted as follows:

$$Z_{t,n}^{\mathcal{S} \rightarrow \mathcal{S}} = Z_{t,n}^{\mathcal{S}*,k} + Z_{t,n}^{\mathcal{S}} \odot (1 - M_{t,n-1}^{\mathcal{S}*,k}), \quad (10)$$

where $Z_{t,n}$ denotes a unified concept for both video and image scenarios, and similarly hereinafter.

Discussion. Through intra-domain mixing, we adaptively generated intra-mixed source domain ($\mathcal{S} \rightarrow \mathcal{S}$) and intra-mixed target domain ($\mathcal{T} \rightarrow \mathcal{T}$). As feature visualization in Fig. 7(b) for video examples, the feature distribution of the latter one is closer to the source domain, and both intra-mixed domains exhibit more generalized feature embeddings. Ablation studies in Table VI demonstrate that our intra-domain mixing outperforms purely alternating training, one-way or two-way mixing across domains. We attribute this to the enriched and continuous distribution of intra-mixed domains, which diminishes the *distinct point attributes* of the naive domains, thus effectively bridging the domain gap and facilitating knowledge transfer.

D. Inter-Mixed Video/Image Domain Adaptation

The feature gap bridging facilitated by intra-mixed domains prompts us to delve deeper into domain-wise interaction. In addition, existing methods [19], [21]–[24], [39], [73] often focus purely on image-level mixing, neglecting the resulting semantic feature inconsistencies. Given our design of video/image patch templates at the pixel level, could we further enhance

feature consistency across quad-mixed domains at the feature level? Driven by this, building upon our intra-mixed domains, we propose more enhanced inter-mixed domains and feature-level mixing, thereby bridging domain gaps comprehensively and alleviating feature inconsistencies.

Formally, we term the outcome of *target to intra-mixed source mixing* as inter-mixed source domain, and vice versa.

1) *Target to Intra-mixed Source Mixing ($\mathcal{T} \rightarrow (\mathcal{S} \rightarrow \mathcal{S})$)*: Following our design, inter-mixed domains should undergo feature-level interaction rather than being trained independently. To achieve this, we also utilize source and target patch templates to create more enhanced inter-mixed domains derived from our intra-domains, enabling the model to learn rich and invariant features across domains. The formula for the target to intra-mixed source domain mixing is as follows:

$$Z_{t,n}^{\mathcal{T} \rightarrow (\mathcal{S} \rightarrow \mathcal{S})} = Z_{t,n}^{\mathcal{T}*,k} + Z_{t,n}^{\mathcal{S} \rightarrow \mathcal{S}} \odot (1 - M_{t,n-1}^{\mathcal{T}*,k}). \quad (11)$$

For **UDA-ISS**, the generated inter-mixed source domain sample is a set that integrates spatial elements. While for **UDA-VSS**, it further involves temporal elements, akin to Eq. (1), which encompasses video frames, labels, and inter-frame optical flow. Notably, the inter-mixed source domain integrates semantics from both source and target domains, featured with a more diverse and enhanced feature embedding space, which can facilitate the domain gap bridging.

2) *Source to Intra-mixed Target Mixing ($\mathcal{S} \rightarrow (\mathcal{T} \rightarrow \mathcal{T})$)*: The generation of the inter-mixed target domain follows a similar approach to Eq. (11):

$$Z_{t,n}^{\mathcal{S} \rightarrow (\mathcal{T} \rightarrow \mathcal{T})} = Z_{t,n}^{\mathcal{S}*,k} + Z_{t,n}^{\mathcal{T} \rightarrow \mathcal{T}} \odot (1 - M_{t,n-1}^{\mathcal{S}*,k}). \quad (12)$$

Compared to the large feature gap between naive source and target domains, the gap between the inter-mixed domains is effectively bridged, as depicted in Fig. 7(a)(e). This facilitates the transfer of rich knowledge learned from the source domain to the target domain, promoting effective domain adaptation.

The partial labels from source domain patch templates within the inter-mixed target domain could aid in learning global features. Additionally, to enhance the diversity of patch templates from two domains, we ensure that categories of cross-domain templates are exclusive.

3) *Feature-Level Template Mixing*: Based on the design that the two inter-mixed domains encompass shared category-aware video/image templates from both the source and target domains, we encourage the model to alleviate *feature inconsistencies* arising from varying domain-specific semantic contexts and prioritize learning domain-invariant features of them.

For **UDA-VSS**, we adaptively perform feature-level template mixing across two inter-mixed domains to enhance the consistency learning of diverse spatio-temporal features, as depicted in Fig. 4(b). Firstly, the feature-level mask sequence $M_{t,n-1}^{\mathcal{D}^*} \downarrow$ is created to map spatio-temporal features from the inter-mixed source domain samples, and then the mapping results are fused with inter-mixed target domain features. The process is as follows:

$$F_{t,n}^{\mathcal{S} \rightarrow (\mathcal{T} \rightarrow \mathcal{T})} = \psi(F_{t,n}^{\mathcal{T} \rightarrow (\mathcal{S} \rightarrow \mathcal{S})} \odot M_{t,n-1}^{\mathcal{D}^*} \downarrow, F_{t,n}^{\mathcal{S} \rightarrow (\mathcal{T} \rightarrow \mathcal{T})}) \odot M_{t,n-1}^{\mathcal{D}^*} \downarrow + F_{t,n}^{\mathcal{S} \rightarrow (\mathcal{T} \rightarrow \mathcal{T})} \odot (1 - M_{t,n-1}^{\mathcal{D}^*} \downarrow), \quad (13)$$

where $F_{t,n}$ denotes the feature stack of adjacent frames, ψ denotes a 1×1 convolution layer, and the category-aware feature binary mask $M_{t,n-1}^{\mathcal{D}^*} \downarrow$ is downsampled from the integrated $M_{t,n-1}^{\mathcal{D}^*}$ using bilinear interpolation. The resolution of $M_{t,n-1}^{\mathcal{D}^*} \downarrow$ is same as F_t , and $M_{t,n-1}^{\mathcal{D}^*}$ is obtained as follows:

$$M_{t,n-1}^{\mathcal{D}^*} = M_{t,n-1}^{\mathcal{S}^*} \cup M_{t,n-1}^{\mathcal{T}^*}, \quad (14)$$

where \mathcal{D} denotes the union of source \mathcal{S} and target \mathcal{T} domain.

For **UDA-ISS**, $F_{t,n}$ corresponding to spatial image features, following a parallel manner.

Discussion. From a unified view, we propose a fairly simple, efficient, and practical solution to bridge video/image feature gaps and alleviate feature inconsistencies, facilitated by quad-mixing at pixel and feature levels. The diverse and rich domain-wise contexts aid in the domain-invariant feature learning, as illustrated in Fig. 1(d) and feature visualization in Fig. 7(e). Notably, we only utilize quad-mixed data ($\mathcal{T} \rightarrow (\mathcal{S} \rightarrow \mathcal{S})$) and ($\mathcal{S} \rightarrow (\mathcal{T} \rightarrow \mathcal{T})$) for training. Compared to incrementally using ($\mathcal{S} \rightarrow \mathcal{S} + \mathcal{T} \rightarrow \mathcal{T} + \mathcal{S} \rightarrow \mathcal{T} + \mathcal{T} \rightarrow \mathcal{S}$), our method yields superior results while reducing computational costs by a large margin. Detailed ablation analysis is provided in Table VI and Table XI.

E. Flow-Guided Feature Aggregation for Domain Alignment

To further mitigate domain gaps for **UDA-VSS**, we propose compressing video features into compact distribution for fine-grained alignment. Unlike only aligning spatial features of one single frame [39], we fully leverage temporal clues to generate cross-frame consistent target pseudo-labels, maintain temporal consistency of spatial features for each domain, and aggregate spatial and temporal features guided by optical flow for fine-grained domain alignment. As a result, aggregated video features from two domains exhibit an aligned and compact distribution, thus enhancing segmentation performance for the target domain. Note that it can also be extended to **UDA-ISS**.

1) *Flow-Guided Spatio-Temporal Feature Extraction*: In this paper, we employ a variant of ACCEL [57] as the basic architecture of video segmentation network, which involves two weight-shared CNN/Transformer-based segmentation branches and an optical flow branch. The segmentation branches capture the spatial feature, using two adjacent frames from the stacked $X_t = \mathbb{S}\{x_{t-1}, x_t\}$ as input. The optical flow $o_{t-1 \rightarrow t}$ is used to propagate temporal information across frames. We conduct feature-level template mixing proposed in Section III-D3 during forward training across inter-mixed domain samples.

For clarity, we illustrate with pure source and target domain in this part, showing that the inter-mixed source and target domain also adhere to the same paradigm. During source and target domain training, the features $F_t = \mathbb{S}\{f_{t-1}, f_t\}$ of adjacent frames are fused to generate holistic feature of frame x_t , leveraging the video temporal continuity, where F represents the deep feature of adjacent frames in this section. Specifically, we feed feature f_t and optical flow-warped feature $f_{t-1 \rightarrow t}$ into a convolutional fusion layer ϕ_f to generate segmentation logits vector $p_{t-1 \rightarrow t}$ (abbreviated as p_t). The process is described as follows:

$$p_{t-1 \rightarrow t} = \phi_f(f_{t-1 \rightarrow t}, f_t), \quad (15)$$

where the optical flow-warped feature $f_{t-1 \rightarrow t}$ is obtained by:

$$f_{t-1 \rightarrow t} = \phi_{\mathcal{W}}(f_{t-1}, o_{t-1 \rightarrow t}), \quad (16)$$

where $\phi_{\mathcal{W}}$ is a warp operation using bilinear interpolation.

For target pseudo-label generation, different from existing UDA-VSS works using a momentum network [21], [22], we employ a cross-frame propagation strategy to maintain the inherent temporal continuity. As shown in the left part of Fig. 2(a), consecutive input set $Z_{t-\tau}^{\mathcal{T}}$ from the target domain are fed into the segmentation network to generate the logits vector $p_{t-\tau}^{\mathcal{T}}$. Then, we yield pseudo-label $\hat{y}_t^{\mathcal{T}}$ by warping $p_{t-\tau}^{\mathcal{T}}$ using optical flow $o_{t-1 \rightarrow t}^{\mathcal{T}}$, as described below:

$$\hat{y}_t^{\mathcal{T}} = \arg \max_k (\phi_{\mathcal{W}}(p_{t-\tau}^{\mathcal{T},(k)}, o_{t-1 \rightarrow t}^{\mathcal{T}})). \quad (17)$$

For target domain testing, as shown in Fig. 2(c), only stacked sets $Z_t^{\mathcal{T}}$ are input to the model to obtain segmentation results.

2) *Spatio-Temporal Feature Aggregation for Domain Alignment*: To further mitigate the video domain gap, we propose adaptive aggregation along spatial and temporal dimensions to reduce the distribution discrepancy of scattered video features. Unlike previous methods [39], [71] only emphasizing image feature discrepancy across domains, we comprehensively consider spatial features of consecutive frames and fully leverage temporal information. In the spatial dimension, fused features $p_{t' \rightarrow t}^{\mathcal{T}}$ that integrate flow-guided features from previous timestamps t' to frame t are adaptively aggregated. For the target domain, we set $t' \in \mathbb{T} = \{t-1, t-\tau, t-\tau-1\}$, while for the source domain, $t' \in \mathbb{T} = \{t-1\}$, benefiting from source label supervision to reduce computational cost.

Specifically, as shown in Fig. 5, we warp frame features for two domains from the previous time step t' to t following Eq. (16) to get the warped feature $f_{t' \rightarrow t}$, respectively. Then, upon merging $f_{t' \rightarrow t}$ with feature f_t through the fusion layer ϕ_f , we generate temporal consistent spatial feature $p_{t' \rightarrow t}^{\mathcal{T}}$ for

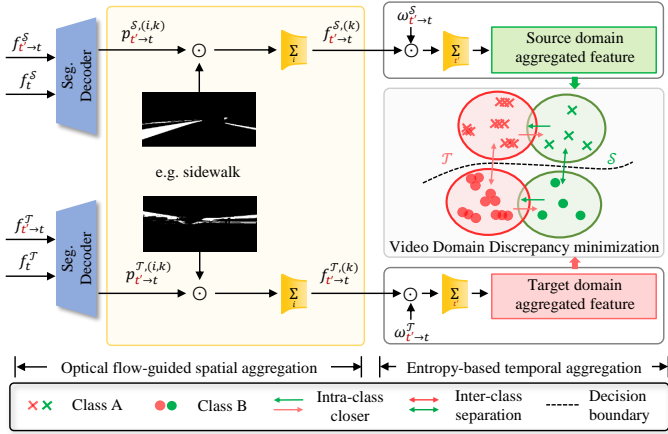


Fig. 5. The illustration of the optical flow-guided spatio-temporal feature aggregation for domain alignment, where t' signifies previous time step, and $\omega_{t'-t}^T$ denotes temporal aggregation weights of target frames. The symbol $p_{t'-t}^{T,(i,k)}$ denotes the optical flow-guided frame feature warped from the previous time step t' , where “ \rightarrow ” denotes the warp direction along the time dimension.

frame t . Based on this, we adaptively distribute the spatial feature to category-aware subspaces by pixel mapping operation in a fine-grained manner. For the target domain, we obtain spatial-aggregated feature $f_{t'-t}^{\mathcal{T},(k)}$ defined as follows:

$$f_{t'-t}^{\mathcal{T},(k)} = \frac{\sum_{i=1}^{H \times W} (p_{t'-t}^{\mathcal{T},(i,k)} \odot \mathbb{1}(\hat{y}_{t'-t}^{\mathcal{T},(i,k)} == k))}{\sum_{i=1}^{H \times W} \mathbb{1}(\hat{y}_{t'-t}^{\mathcal{T},(i,k)} == k)}, \quad (18)$$

where k belongs to the whole category space. And source spatial-aggregated feature $f_{t'-t}^{\mathcal{S},(k)}$ follows a similar manner. In this way, adaptive aggregation along the spatial dimension across two domains is conducted in a fine-grained way.

Based on this, we conducted temporal aggregation by assembling spatial-aggregated features from consecutive frames using an entropy confidence [74] $\omega_{t'-t}^{\mathcal{T}}$, for the target domain:

$$f^{\mathcal{T},(k)} = \sum_{t' \in \mathcal{T}} f_{t'-t}^{\mathcal{T},(k)} \cdot \omega_{t'-t}^{\mathcal{T}}, \quad (19)$$

where $\omega_{t'-t}^{\mathcal{T}}$ is obtained by softmax normalization of logits entropy among the fused spatial features, formulated as:

$$\omega_{t'-t}^{\mathcal{T}} = \text{softmax}_{t'} \left(-\frac{1}{H \times W} \sum_i^{H \times W} (-p_{t'-t}^{\mathcal{T},(i)} \cdot \log(p_{t'-t}^{\mathcal{T},(i)})) \right), \quad (20)$$

where the segmentation confidence and temporal weight $\omega_{t'-t}^{\mathcal{T}}$ are promoted to be positively correlated.

Subsequently, we concatenate the aggregated video features along the category level for two domains to generate fine-grained video features, where the concatenation is denoted as \mathbb{C}_k . In this paper, we propose mitigating the fine-grained video feature gap using MMD (Maximum Mean Discrepancy) [29] minimization, benefiting from the optical flow-guided temporal information propagation and distribution alignment.

As for **UDA-ISS**, spatial aggregation can be used for fine-grained alignment without relying on temporal clues, i.e., optical flow guidance.

F. Training Procedure and Objective Optimization

Our method follows a self-supervised learning paradigm trained end-to-end. The training algorithm is summarized in supplementary materials. The overall loss is defined as follows:

$$\mathcal{L}_{all} = \mathcal{L}_{QuadMix} + \mathcal{L}_{Agg} + \mathcal{L}_{SSL}. \quad (21)$$

For **UDA-VSS**, specific losses are denoted as follows:

QuadMix loss. As shown in Fig. 4, the loss for quad-directional mixing used for gap bridging is as follows:

$$\mathcal{L}_{QuadMix} = \mathcal{L}_{CE}^{S'}(\mathcal{G}(X_t^{S'}, o_{t-1 \rightarrow t}^{S'}, y_t^{S'})) + \lambda_{\mathcal{T}} \mathcal{L}_{CE}^{\mathcal{T}'}(\mathcal{G}(\mathcal{A}(X_t^{\mathcal{T}'}, o_{t-1 \rightarrow t}^{\mathcal{T}'}, \hat{y}_t^{\mathcal{T}'}))), \quad (22)$$

where \mathcal{G} denotes the video semantic segmentation network, \mathcal{A} means image enhancement, \mathcal{L}_{CE} denotes cross-entropy loss, and \mathcal{S}' and \mathcal{T}' indicate two inter-mixed domains for simplicity.

Aggregated feature alignment loss. We define the following loss to minimize the discrepancy of aggregated spatio-temporal feature distribution across domains:

$$\mathcal{L}_{Agg} = \lambda_f \left\| \mathbb{E}(\mathbb{C}_k(f^{\mathcal{S},(k)})) - \mathbb{E}(\mathbb{C}_k(f^{\mathcal{T},(k)})) \right\|_{\mathcal{H}}^2 \quad (23)$$

Self-supervised learning loss. We also employ a cross-domain self-supervised learning loss for two video domains:

$$\mathcal{L}_{SSL} = \mathcal{L}_{CE}^{\mathcal{S}}(\mathcal{G}(X_t^{\mathcal{S}}, o_{t-1 \rightarrow t}^{\mathcal{S}}, y_t^{\mathcal{S}})) + \lambda_{\mathcal{T}} \mathcal{L}_{CE}^{\mathcal{T}}(\mathcal{G}(\mathcal{A}(X_t^{\mathcal{T}}, o_{t-1 \rightarrow t}^{\mathcal{T}}, \hat{y}_t^{\mathcal{T}}))). \quad (24)$$

For **UDA-ISS**, the model’s input in Eq. (22) and Eq. (24) should be replaced by a single image. Moreover, the sensitivity analysis for hyperparameters $\lambda_{\mathcal{T}}$ and λ_f will be specifically discussed in the experiments.

IV. EXPERIMENTS

A. Experimental Setups

1) **UDA-VSS Benchmark:** We conduct experiments on two challenging benchmarks: Synthia-Seq [8] \rightarrow Cityscapes-Seq [7] and VIPER [9] \rightarrow Cityscapes-Seq. **Cityscapes-Seq** (target domain) includes real city scene videos from 50 cities in Germany and neighboring countries. It comprises 2,975 training video clips and 500 validation video clips, and each clip contains continuous 30 frames. **Synthia-Seq** (source domain) contains 8,000 photo-realistic frames with dense labels. We use frames in the *RGB* folder and choose 11 categories for adaptation. **VIPER** (source domain) is another challenging synthetic video dataset, consisting of 133,670 frames of virtual videos rendered from urban landscape scenes in the virtual computer game “Grand Theft Auto V”. We use 13,367 frames with segmentation labels as another source domain, choosing 15 categories for adaptation. Our dataset setting is consistent with previous works [6], [36]–[39], [71], [75], etc.

2) **UDA-ISS Benchmark:** We conduct experiments on two popular benchmarks GTAV [10] \rightarrow Cityscapes and Synthia [8] \rightarrow Cityscapes. **Cityscapes** (target domain) is a subset of Cityscapes-Seq, with each image being the 20-th frame of each corresponding video clip. **GTAV** (source domain) is a synthetic image dataset with labels for semantic segmentation, where images are also collected from “Grand Theft Auto V.” It comprises 19 categories common with Cityscapes

TABLE I

COMPARISON FOR **UDA-VSS** ON SYNTHIA-SEQ \rightarrow CITYSCAPES-SEQ. THE BEST RESULTS ARE IN **BOLD**, AND THE SUBOPTIMAL RESULTS ARE IN UNDERLINED. “ADV.”: ADVERSARIAL LEARNING, “SSL”: SELF-SUPERVISED LEARNING, “WARM”: WARM-UP, “TRANS.”: TRANSFORMER-BASED NETWORK. \dagger DENOTES RETRAINED RESULTS OF IMAGE DOMAIN METHODS USING A VIDEO SEGMENTATION BACKBONE [57] FOR FAIR COMPARISON.

Methods	Adv.	SSL	Warm	Road	Side.	Buil.	Pole	Light	Sign	Vege.	Sky	Pers.	Rider	Car	mIOU
Source-Only				56.3	26.6	75.6	25.5	5.7	15.6	71.0	58.5	41.7	17.1	27.9	38.3
AdvEnt \dagger [11]	✓			85.7	21.3	70.9	21.8	4.8	15.3	59.5	62.4	46.8	16.3	64.6	42.7
CBST \dagger [12]		✓		64.1	30.5	78.2	28.9	14.3	21.3	75.8	62.6	46.9	20.2	33.9	43.3
IDA \dagger [13]	✓			87.0	23.2	71.3	22.1	4.1	14.9	58.8	67.5	45.2	17.0	73.4	44.0
CRST \dagger [14]		✓		70.4	31.4	79.1	27.6	11.5	20.7	78.0	67.2	49.5	17.1	39.6	44.7
SVMin \dagger [15]				84.9	0.5	77.9	29.6	7.4	15.0	78.6	73.2	46.9	6.2	73.8	44.9
CrCDA \dagger [16]	✓			86.5	26.3	74.8	24.5	5.0	15.5	63.5	64.4	46.0	15.8	72.8	45.0
RDA \dagger [17]		✓		84.7	26.4	73.9	23.8	7.1	18.6	66.7	68.0	48.6	9.3	68.8	45.1
FDA \dagger [18]		✓		84.1	32.8	67.6	28.1	5.5	20.3	61.1	64.8	43.1	19.0	70.6	45.2
SAC \dagger [5]		✓		87.0	41.1	64.0	20.4	12.1	32.8	38.2	47.6	53.1	19.3	81.1	45.2
DACS \dagger [19]		✓		86.4	40.0	74.0	27.8	9.5	28.2	71.6	72.0	55.6	20.0	76.4	51.0
PixMatch \dagger [20]		✓		90.2	<u>49.9</u>	75.1	23.1	17.4	34.2	67.1	49.9	55.8	14.0	84.3	51.0
DA-VSN [6]	✓			89.4	31.0	77.4	26.1	9.1	20.4	75.4	74.6	42.9	16.1	82.4	49.5
I2VDA [71]		✓		89.9	40.5	77.6	27.3	18.7	23.6	76.1	76.3	48.5	22.4	82.1	53.0
TPS [37]		✓		91.2	53.7	74.9	24.6	17.9	39.3	68.1	59.7	57.2	20.3	84.5	53.8
SFC [38]		✓		90.9	32.5	76.8	28.6	6.0	36.7	76.0	78.9	51.7	13.8	85.6	52.5
TPL-SFC [38]		✓		90.0	32.8	80.4	28.9	14.9	35.3	80.8	81.1	57.5	19.6	86.7	55.3
PAT [75]		✓		<u>91.5</u>	41.3	76.1	29.6	20.9	33.8	72.4	75.9	51.3	24.7	86.2	54.9
CMOM [39]		✓	✓	90.4	39.2	82.3	30.2	16.3	29.6	83.2	<u>84.9</u>	59.3	19.7	84.3	56.3
QuadMix		✓		90.5	41.2	81.1	29.3	23.1	47.5	82.7	83.8	61.1	28.4	87.0	59.6
QuadMix		✓	✓	90.8	39.9	83.2	<u>33.2</u>	<u>30.1</u>	<u>50.7</u>	84.8	82.3	<u>61.2</u>	<u>32.7</u>	87.4	61.5
QuadMix (Trans.)		✓		94.1	61.9	<u>82.9</u>	36.9	41.0	59.1	85.2	85.6	64.3	37.8	90.3	67.2

and 24,966 labeled images. **Synthia** (source domain) is another synthetic image dataset, we use images from the SYNTHIARAND-CITYSCAPES folder which contains 9,400 images and 16 common categories with Cityscapes, akin to previous works [19], [21]–[23], [73], [76], [77], etc.

3) *Implementation Details*: Our model is implemented in PyTorch and trained on a single NVIDIA Tesla V100 GPU. The details are as follows: (i) As for the network, we employ a variant of ACCEL [57] for UDA-VSS, using DeepLabV2 [78] or MiT-B5 in DAformer [24] as the segmentation branch, and FlowNet [79] as the optical flow branch. For UDA-ISS, we only employ the segmentation branch. Notably, DeepLabV2 uses ResNet-101 [80] as its backbone, and both DeepLabV2 and MiT-B5 are pre-trained on ImageNet [81]; (ii) As for input resolution, for video tasks, we resize the resolution of Cityscapes-Seq, Synthia-Seq, and VIPER to 1024×512 , 760×1280 , and 720×1280 , respectively. While for image tasks, images undergo resizing to dimensions of 720×1280 , 512×1024 , and 760×1280 for Cityscapes, GTAV, and Synthia; (iii) We set batch size B to 1 for video and 2 for image scenarios; (iv) For DeepLabV2, we use the SGD optimizer with a momentum of 0.9 and a weight decay of 5×10^{-4} . The initial learning rate is 2.5×10^{-4} for Synthia-Seq to Cityscapes-Seq and two image benchmarks, and 1×10^{-4} for VIPER to Cityscapes-Seq. For transformer networks, we use an AdamW optimizer with a weight decay of 0.01 and betas set to (0.9, 0.999). The learning rate is initially set to 6×10^{-5} for the encoder and 6×10^{-4} for the decoder, with a linear warmup followed by linear decay; (v) Our models are trained for a maximum of 40k iterations for four benchmarks; (vi)

Other issues: we apply Gaussian blur and color jitter to the target domain for image enhancement. Aligned with [6], [37], [39], we set video temporal deviation τ to 1. Additionally, the confidence threshold for target filtering operation \mathcal{F} is 0.9. During quad-directional mixing, source videos undergo random cropping to match the resolution of target videos. For image tasks, we set $\lambda_{\mathcal{T}}$ and λ_f to 1 for simplicity; (vii) In this paper, we use per-category IOU (Intersection over Union) and mIOU (mean IOU) as evaluation metrics. Experiment settings are consistent with prior works for fair comparison.

B. Experimental Results

1) *Comparison With State-of-the-Arts of UDA-VSS*: In Table I and Table II, we compare our method with the state-of-the-art methods on Synthia-Seq \rightarrow Cityscapes-Seq and VIPER \rightarrow Cityscapes-Seq benchmark. To the best of our knowledge, recent methods [6], [36]–[39], [71], [75] are the most superior works in UDA-VSS, all employing CNN architectures. In this paper, we also explore *transformer-based networks* for the first time. Moreover, we also compare several variants to UDA-VSS that are initially designed for UDA-ISS, including works [5], [11]–[20]. Technically, following previous UDA-VSS works [6], [37], [39], [71], we replace their image segmentation backbones with a video segmentation network (denoted by \dagger). Additionally, “Adv.” signifies methods that employ adversarial learning, and “SSL” denotes self-supervised learning. “Warm” denotes model parameter initialization using a warm-up model. “Trans.” denotes the transformer backbone, while others use ResNet-101 pre-trained on ImageNet.

TABLE II

COMPARISON FOR **UDA-VSS** ON VIPER \rightarrow CITYSCAPES-SEQ. THE BEST RESULTS ARE IN **BOLD**, AND THE SUBOPTIMAL RESULTS ARE IN UNDERLINED. “ADV.”: ADVERSARIAL LEARNING, “SSL”: SELF-SUPERVISED LEARNING, “WARM”: WARM-UP, “TRANS.”: TRANSFORMER-BASED NETWORK. \dagger DENOTES RETRAINED RESULTS OF IMAGE DOMAIN METHODS USING A VIDEO SEGMENTATION BACKBONE [57] FOR FAIR COMPARISON.

Methods	Adv.	SSL	Warm	Road	Side.	Buil.	Fenc.	Light	Sign	Vege.	Terr.	Sky	Pers.	Car	Truc.	Bus	Mot.	Bike	mIOU
Source-Only	✓			56.7	18.7	78.7	6.0	22.0	15.6	81.6	18.3	80.4	55.9	66.3	4.5	16.8	20.4	10.3	37.1
AdvEnt [†] [11]	✓			78.5	31.0	81.5	22.1	29.2	26.6	81.8	13.7	80.5	58.3	64.0	6.9	38.4	4.6	1.3	41.2
CBST [†] [12]		✓		48.1	20.2	84.8	12.0	20.6	19.2	83.8	18.4	84.9	59.2	71.5	3.2	38.0	23.8	37.7	41.7
IDA [†] [13]	✓			78.7	33.9	82.3	22.7	28.5	26.7	82.5	15.6	79.7	58.1	64.2	6.4	41.2	6.2	3.1	42.0
CRST [†] [14]		✓		56.0	23.1	82.1	11.6	18.7	17.2	85.5	17.5	82.3	60.8	73.6	3.6	38.9	30.5	35.0	42.4
SVMin [†] [15]				51.1	14.3	80.8	11.9	30.9	23.1	83.5	<u>37.7</u>	74.5	59.5	79.7	36.4	<u>53.2</u>	20.0	4.2	44.1
CrCDA [†] [16]	✓			78.1	33.3	82.2	21.3	29.1	26.8	82.9	28.5	80.7	59.0	73.8	16.5	41.4	7.8	2.5	44.3
RDA [†] [17]		✓		72.0	25.9	80.8	15.1	27.2	20.3	82.6	31.4	82.2	56.3	75.5	22.8	48.3	19.1	6.7	44.4
FDA [†] [18]		✓		70.3	27.7	81.3	17.6	25.8	20.0	83.7	31.3	82.9	57.1	72.2	22.4	49.0	17.2	7.5	44.4
DACS [†] [19]		✓		69.6	24.1	76.9	9.1	16.1	15.3	74.1	20.3	76.5	59.4	74.8	38.6	43.1	7.7	1.9	40.5
SAC [†] [5]		✓		52.2	19.6	73.4	3.7	23.1	25.2	73.9	17.3	78.1	56.9	80.3	38.3	48.2	17.8	14.1	41.5
PixMatch [†] [20]		✓		79.4	26.1	84.6	16.6	28.7	23.0	85.0	30.1	83.7	58.6	75.8	34.2	45.7	16.6	12.4	46.7
DA-VSN [6]	✓			86.8	36.7	83.5	22.9	30.2	27.7	83.6	26.7	80.3	60.0	79.1	20.3	47.2	21.2	11.4	47.8
TPS [37]		✓		82.4	36.9	79.5	9.0	26.3	29.4	78.5	28.2	81.8	61.2	80.2	39.8	40.3	28.5	31.7	48.9
MoDA [36]		✓		72.2	25.9	80.9	18.3	24.6	21.1	79.1	23.2	78.3	68.7	84.1	43.2	49.5	28.8	38.6	49.1
I2VDA [71]		✓		84.8	36.1	84.0	28.0	<u>36.5</u>	36.0	<u>85.9</u>	32.5	74.0	63.2	81.9	33.0	51.8	39.9	0.1	51.2
SFC [38]		✓		89.9	40.8	83.8	6.8	34.4	25.0	85.1	34.3	84.1	62.6	82.1	35.3	47.1	23.2	31.3	51.1
TPL-SFC [38]		✓		89.9	41.5	84.0	7.0	<u>36.5</u>	27.1	85.6	33.7	<u>86.6</u>	62.4	82.6	36.3	47.6	23.2	31.9	51.7
PAT [75]		✓		85.3	42.3	82.5	25.5	33.7	36.1	86.6	32.8	84.9	61.5	83.3	34.9	46.9	29.3	29.9	53.0
CMOM [39]		✓	✓	89.0	53.8	86.8	31.0	32.5	47.3	85.6	25.1	80.4	65.1	79.3	21.6	43.4	25.7	40.6	53.8
QuadMix		✓		91.4	43.5	85.5	21.3	26.6	40.2	84.7	34.2	84.6	62.1	84.3	39.9	46.6	33.5	45.6	54.9
QuadMix		✓	✓	91.6	51.4	<u>87.0</u>	24.1	32.3	37.2	84.1	28.4	84.8	64.4	<u>85.7</u>	<u>41.4</u>	46.5	34.0	<u>49.6</u>	<u>56.2</u>
QuadMix (Trans.)		✓		87.3	43.8	87.3	25.2	40.0	36.9	86.7	20.8	90.3	65.8	86.8	48.6	65.6	37.6	49.7	58.2

Synthia-Seq \rightarrow Cityscapes-Seq. In Table I, we present experimental results comparing our method with state-of-the-art techniques on the Synthia-Seq \rightarrow Cityscapes-Seq. For clarity, the best per-category IOU and mIOU results are in bold, while suboptimal results are underlined. We observed that: (i) Our method is compatible with both CNN and transformer-based architectures. The proposed CNN-based Quadmix significantly outperforms the previous best CMOM [39] by 5.2% mIOU. When equipped with a transformer, we further boost mIOU by 5.7%, achieving the highest result of 67.2%; (ii) For CNN-based QuadMix, without a warm-up model, we achieved 59.6% mIOU, which is 4.3% higher than TPL-SFC [38] by a large margin. When using a warm-up model, we outperform the CMOM [39] by 5.2%, which relies heavily on the warm-up model [6] for both model initialization and pseudo-label generation; (iii) Adversarial learning methods can improve the model’s adaptation but are less improving compared to self-supervised methods; (iv) Our method boosts the IOU for most categories, which can be attributed to our comprehensive quad-directional mixing, which effectively addresses distinct point attributes and feature inconsistencies, as well as flow-guided video feature aggregation for cross-domain alignment.

Viper \rightarrow Cityscapes-Seq. The domain gap between Viper and Cityscapes-Seq is much larger than that of Synthia-Seq and Cityscapes-Seq. As shown in Table II, our proposed QuadMix also achieves state-of-the-art results. We can conclude that: (i) For CNN-based QuadMix, we achieve 56.2% mIOU with a warm-up model and 54.9% mIOU without it; further-

more, we obtain 58.2% mIOU when we employ transformer-based network. All our results significantly outperform previous methods; (ii) Recent work I2VDA [71] focuses exclusively on transferring source spatial information to target domain videos, resulting in a target domain mIOU of 51.7%. This is inferior to our model, which comprehensively investigates both spatial and temporal level domain shifts. (iii) Variants of image domain adaptation methods generally underperform on target videos compared to UDA-VSS methods, likely due to inadequate utilization of crucial temporal information.

Qualitative results comparison on two benchmarks. In Fig. 6, we present adjacent three frames and corresponding qualitative segmentation results of our method along with the source-only model, DA-VSN [6], TPS [37], and CMOM [39] on Cityscape-Seq validation dataset. Notably, it only offers a ground-truth label for the 19-th frame of each 30-frame video clip, so we replicate the label from frame t for frames $t-1$ and $t+1$, marked with red borders for clarity. Our results exhibit smoother edges and refined details. For example, on Synthia-Seq \rightarrow Cityscapes-Seq benchmark, we obtain more accurate segmentation for categories like *person*, *sign*, and *sidewalk*. Similarly, in the case of Viper \rightarrow Cityscapes-Seq, our model predicts contours that closely resemble actual *bicycle* and *person*, indicating a significant improvement. Please refer to the [supplementary video](#) for more visual comparisons.

2) *Comparison With State-of-the-Arts of UDA-ISS:* For UDA-ISS, we replace spatio-temporal QuadMix with spatial QuadMix, and substitute optical guided spatio-temporal ag-

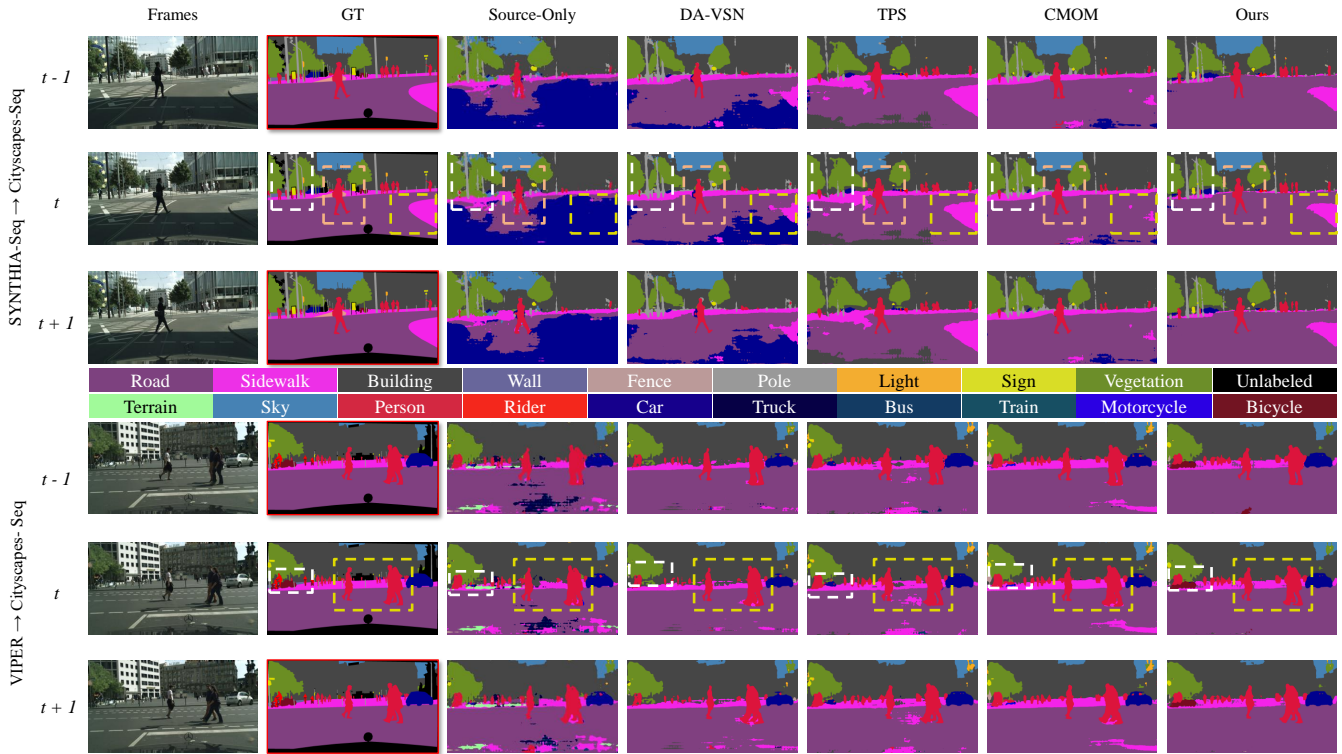


Fig. 6. Qualitative results for three consecutive frames from the Cityscapes-Seq validation set. The results are presented in the following order: target image, ground truth, semantic segmentation results from source-only model, DA-VSN [6], TPS [37], CMOM [39], and the proposed method. We achieve the highest segmentation accuracy, exhibiting smoother edges and refined details. Please zoom in for details.

gregation with spatial aggregation for fine-grained alignment. Technically, we shift elements of $Z_{t,n}^{S*,k}$ and $Z_{t,n}^{T*,k}$ as defined in Section III-B, and remove the reliance on temporal clues that are not present in image scenarios. Additionally, target pseudo-labels are generated using a momentum network [72].

Table III and Table IV compare our method with existing UDA-ISS approaches. Impressively, we maintain superiority on two challenging benchmarks: GTAV \rightarrow Cityscapes and Synthia \rightarrow Cityscapes. We compare with recent advanced CNN-based methods [5], [17], [19]–[23], [73], [76], [77] and transformer-based methods [23], [24], [77]. Notably, DACS [19] proposes one-way mixing, which is followed by subsequent works [23], [24], [77] combining contrastive learning or long-tail learning. Other works [21], [22] employ two-way mixing, with the latter integrating style transfer. However, as analyzed above, they overlooked distinct point attributes within each domain, leading to fragmentary and insufficient domain gap bridging. Additionally, their focus on pixel-level mixing alone can result in feature inconsistencies, hindering effective knowledge transfer. In contrast, we address these challenges comprehensively and obtain remarkable results.

GTAV \rightarrow Cityscapes. As shown in Table III, our method achieves mIOUs of 66.8% with DeepLab-V2 and 76.1% with transformer networks. Notably, QuadMix (Trans.) more effectively extracts spatial features from long-tail categories. Specifically, for the *train* class, our method achieves an IOU of 82.3%, surpassing that of FREDOM [77] (72.5%), which is tailored for long-tail learning. Notably, QuadMix (DL-

V2) underperforms for the *train* class due to the limited feature extraction capability of CNNs. We believe that more frequent resampling of such categories could improve the results. Generally, our method boosts the performance of most categories, exhibiting robust improvement.

Synthia \rightarrow Cityscapes. In Table IV, we present results for 13-category (mIOU*) and 16-category (mIOU) adaptation, following [22], [23], etc. BDM [21] only studies 13-category adaption. Our method consistently outperforms previous works and is well-adapted for transformers and particularly CNN networks on this benchmark, validating its effectiveness.

C. Ablation Study

In this section, we conduct ablation studies to validate quad-directional mixing and flow-guided feature aggregation, using the Deeplabv2 backbone for UDA-VSS tasks by default.

1) *Ablation Study on Each Component:* In Table V, we conduct ablation experiments to verify the effectiveness of three key components: video patch templates (V-tmpl) mixing, feature-level templates (F-tmpl) mixing, and optical-guided video feature aggregation (Agg.). Additionally, we also study the impact of the warm-up mentioned in Table I and Table II. For a fair comparison, we take the results of TPS [37] without random scale augmentation as the baseline (Exp. ID 0*).

It can be concluded that: (i) Video patch templates (V-tmpl) $Z_{t,n}^{*,k}$ result in a 3.70% mIOU gain in Exp. ID 1; (ii) As for feature-level template mixing (F-tmpl) across two enhanced inter-mixed domains, Exp. ID 2 further incorporating

TABLE III

COMPARISON FOR UDA-ISS TASK ON GTAV → CITYSCAPES USING DEEPLAB-V2 (DL-V2) AND TRANSFORMER (TRANS.). THE BEST RESULTS USING TRANS. ARE IN **BOLD**, AND THE BEST RESULTS USING DL-V2 ARE IN UNDERLINED.

Methods	Network	Road	Side.	Buil.	Wall	Fence	Pole	Light	Sign	Vege.	Terr.	Sky	Pers.	Rider	Car	Truck	Bus	Train	Moto.	Bike	mIOU
Source-Only	DL-V2	63.3	15.7	59.4	8.6	15.2	18.3	26.9	15.0	80.5	15.3	73.0	51.0	17.7	59.7	28.2	33.1	3.5	23.2	16.7	32.9
PixMatch [20]	DL-V2	91.6	51.2	84.7	37.3	29.1	24.6	31.3	37.2	86.5	44.3	85.3	62.8	22.6	87.6	38.9	52.3	0.7	37.2	50.0	50.3
RDA [17]	DL-V2	93.1	55.0	84.7	33.1	29.5	38.7	49.3	44.9	84.8	41.6	80.2	62.3	33.2	85.6	37.3	51.3	18.5	34.6	45.3	52.8
DACS [19]	DL-V2	89.9	39.7	87.9	39.7	39.5	38.5	46.4	52.8	88.0	44.0	88.8	67.2	35.8	84.5	45.7	50.2	0.0	27.3	34.0	52.1
SAC [5]	DL-V2	90.4	53.9	86.6	42.4	27.3	45.1	48.5	42.7	87.4	40.1	86.1	67.5	29.7	88.5	49.1	54.6	9.8	26.6	45.3	53.8
DSP [73]	DL-V2	92.4	48.0	87.4	33.4	35.1	36.4	41.6	46.0	87.7	43.2	89.8	66.6	32.1	89.9	57.0	56.1	0.0	44.1	57.8	55.0
BDM [21]	DL-V2	91.3	51.8	86.7	49.9	49.2	53.3	43.1	43.3	85.5	47.9	85.7	62.3	45.9	87.8	55.5	54.4	4.4	46.3	50.4	57.6
I2F [76]	DL-V2	90.8	48.7	85.2	30.6	28.0	33.3	46.4	40.0	85.6	39.1	88.1	61.8	35.0	86.7	46.3	55.6	11.6	44.7	54.3	53.3
ADPL [22]	DL-V2	93.4	60.6	87.5	45.3	32.6	37.3	43.3	55.5	87.2	44.8	88.0	64.5	34.2	88.3	52.6	61.8	49.8	41.8	59.4	59.4
SePiCo [23]	DL-V2	95.2	67.8	88.7	41.4	38.4	43.4	55.5	63.2	88.6	46.4	88.3	73.1	49.0	91.4	63.2	60.4	0.0	45.2	60.0	61.0
FREDDOM [77]	DL-V2	90.9	54.1	87.8	44.1	32.6	45.2	51.4	57.1	88.6	42.6	89.5	68.8	40.0	89.7	58.4	62.6	<u>55.3</u>	47.7	40.0	61.3
QuadMix	DL-V2	<u>97.1</u>	<u>78.0</u>	<u>90.4</u>	<u>49.7</u>	<u>40.3</u>	<u>53.4</u>	<u>61.7</u>	<u>70.9</u>	<u>90.7</u>	<u>49.7</u>	<u>92.9</u>	<u>77.9</u>	<u>53.9</u>	<u>93.5</u>	<u>72.4</u>	<u>65.9</u>	0.7	<u>60.5</u>	<u>68.5</u>	<u>66.8</u>
DAFormer [24]	Trans.	95.7	70.2	89.4	53.5	48.1	49.6	55.8	59.4	89.9	47.9	92.5	72.2	44.7	92.3	74.5	78.2	65.1	55.9	61.8	68.3
SePiCo [23]	Trans.	96.7	76.7	89.7	55.5	49.5	53.2	60.0	64.5	90.2	50.3	90.8	74.5	44.2	93.3	77.0	79.5	63.6	61.0	65.3	70.3
FREDDOM [77]	Trans.	96.7	74.8	90.9	58.1	49.0	57.5	63.4	71.4	91.6	52.1	94.4	78.4	53.1	94.1	83.9	85.2	72.5	62.8	68.9	73.6
QuadMix	Trans.	97.5	80.9	91.6	62.3	57.6	58.2	64.5	71.2	91.7	52.3	94.3	80.0	55.9	94.6	86.3	90.5	82.3	65.1	68.1	76.1

TABLE IV

COMPARISON FOR UDA-ISS TASK ON SYNTHIA → CITYSCAPES USING DEEPLAB-V2 (DL-V2) AND TRANSFORMER (TRANS.). THE BEST RESULTS USING TRANS. ARE IN **BOLD**, AND THE BEST RESULTS USING DL-V2 ARE IN UNDERLINED. mIOU* DENOTES 13-CATEGORY ADAPTATION WITHOUT THREE CLASSES MARKED BY *, WHILE mIOU MEANS 16-CATEGORY ADAPTATION.

Methods	Network	Road	Side.	Buil.	Wall*	Fence*	Pole*	Light	Sign	Vege.	Sky	Pers.	Rider	Car	Bus	Moto.	Bike	mIOU	mIOU*
Source-Only	DL-V2	36.3	14.6	68.8	9.2	0.2	24.4	5.6	9.1	69.0	79.4	52.5	11.3	49.8	9.5	11.0	20.7	33.7	29.5
PixMatch [20]	DL-V2	92.5	54.6	79.8	4.8	0.1	24.1	22.8	17.8	79.4	76.5	60.8	24.7	85.7	33.5	26.4	54.4	46.1	54.5
RDA [17]	DL-V2	89.4	39.0	79.8	8.1	1.2	33.0	22.6	28.1	81.8	82.0	60.9	30.1	82.7	41.4	37.5	48.9	47.9	55.7
DACS [19]	DL-V2	80.6	25.1	81.9	21.5	2.9	37.2	22.7	24.0	83.7	90.8	67.6	38.3	82.9	38.9	28.5	47.6	48.3	54.8
SAC [5]	DL-V2	89.3	47.2	85.5	26.5	1.3	43.0	45.5	32.0	87.1	89.3	63.6	25.4	86.9	35.6	30.4	53.0	52.6	59.3
DSP [73]	DL-V2	86.4	42.0	82.0	2.1	1.8	34.0	31.6	33.2	87.2	88.5	64.1	31.9	83.8	64.4	28.8	54.0	51.0	59.9
BDM [21]	DL-V2	91.0	55.8	86.9	-	-	-	58.3	44.7	85.8	85.7	84.1	40.3	86.0	55.2	45.0	50.6	-	66.8
I2F [76]	DL-V2	84.9	44.7	82.2	9.1	1.9	36.2	42.1	40.2	83.8	84.2	68.9	35.3	83.0	49.8	30.1	52.4	51.8	60.1
ADPL [22]	DL-V2	86.1	38.6	85.9	29.7	1.3	36.6	41.3	47.2	85.0	90.4	67.5	44.3	87.4	57.1	43.9	51.4	55.9	63.6
SePiCo [23]	DL-V2	77.0	35.3	85.1	23.9	3.4	38.0	51.0	55.1	85.6	80.5	73.5	46.3	87.6	<u>69.7</u>	50.9	66.5	58.1	66.5
FREDDOM [77]	DL-V2	86.0	46.3	87.0	<u>33.3</u>	<u>5.3</u>	48.7	38.1	46.8	87.1	<u>89.1</u>	71.2	38.1	87.1	54.6	51.3	59.9	59.1	66.0
QuadMix	DL-V2	<u>88.5</u>	<u>52.9</u>	<u>87.1</u>	3.7	1.4	<u>56.2</u>	<u>62.7</u>	<u>59.2</u>	<u>87.2</u>	89.0	<u>79.1</u>	<u>55.8</u>	<u>87.9</u>	66.7	<u>58.1</u>	<u>71.2</u>	<u>62.6</u>	<u>72.3</u>
DAFormer [24]	Trans.	84.5	40.7	88.4	41.5	6.5	50.0	55.0	54.6	86.0	89.8	73.2	48.2	87.2	53.2	53.9	61.7	60.9	67.4
SePiCo [23]	Trans.	87.0	52.6	88.5	40.6	10.6	49.8	57.0	55.4	56.8	86.2	75.4	52.7	92.4	78.9	53.0	62.6	64.3	71.4
FREDDOM [77]	Trans.	89.4	50.8	89.3	48.8	9.3	57.3	65.1	60.1	89.9	93.7	79.4	51.6	90.5	66.0	62.3	68.1	67.0	73.6
QuadMix	Trans.	88.1	51.2	88.9	46.7	7.9	58.6	64.7	63.7	88.1	93.9	81.3	56.6	90.3	66.9	66.8	66.0	67.5	74.3

F-tmpl demonstrates a 1.54% mIOU gain. In addition, Exp. 8 outperforms Exp. 7 by 1.22%, also validating the efficacy of “F-tmpl”; (iii) In another line, Exp. 3 introduces the optical-guided video feature aggregation (Agg.), resulting in growth to 54.01%; (iv) Furthermore, Exp. ID 4 combines “V-tmpl”, “F-tmpl”, and “Agg.”, achieving an mIOU of 59.62%, surpassing the state-of-the-art TPL-SFC [38] mIOU of 55.3% by 4.32%; (v) Moreover, we also employ the warm-up setup in Exp. ID 5 to Exp. ID 8 for model parameter initialization, exceeding the state-of-the-art CMOM of 56.31% with a warm-up stage by 5.17%, resulting in the highest mIOU of 61.48%, a remarkable 9.47% increase compared to the baseline Exp. ID 0*.

Further comparison. To valid the video patch templates (V-tmpl) $Z_{t,n}^{*,k}$ in Exp. ID 1, we perform a variant using image

patch templates (I-tmpl) akin to [19], [21]. Thus, the model input is also substituted with x_t^S and x_t^T in Eq. (22). It is observed that with “I-tmpl”, the mIOU dropped by 1.37% compared with Exp. ID 1, which suggests that “V-tmpl” enhances the video adaptation more effectively.

Qualitative results of each component. In Fig. 8, we present segmentation results of three adjacent frames on Synthia-Seq → Cityscapes-Seq, following experiment settings corresponding to Exp. ID 0*, ID 2, ID 3, ID 5, ID 8 in Table V. These results demonstrate the incremental integration of each component. The segmentation results progressively improve from left to right, particularly for categories like *sign* and *car*. Notably, the challenging issue with a *person* on the far left within the frame is effectively addressed by integrating the

TABLE V

ABLATION STUDIES ON SYNTHIA-SEQ \rightarrow CITYSCAPES-SEQ. ALL MODELS ARE TRAINED END-TO-END FOR A TOTAL OF 40K ITERATIONS. “V-TMPL” REPRESENTS OUR VIDEO PATCH TEMPLATE AS DEFINED IN EQ. (1). “F-TMPL” DENOTES FEATURE-LEVEL TEMPLATE MIXING ACROSS TWO ENHANCED INTER-MIXED DOMAINS, “AGG” REFERS TO THE OPTICAL-GUIDED VIDEO FEATURE AGGREGATION, “WARM” MEANS INITIALIZING MODEL PARAMETERS USING A WARM-UP MODEL.

ID	SSL	V-tmpl	F-tmpl	Agg.	Warm	mIOU (Gain)
0*	✓					52.01
1	✓	✓				55.71 (+3.70)
2	✓	✓	✓			57.25 (+5.24)
3	✓			✓		54.01 (+2.00)
4	✓	✓	✓	✓		59.62 (+7.61)
5	✓	✓	✓		✓	57.95 (+5.95)
6	✓			✓	✓	55.97 (+3.96)
7	✓	✓		✓	✓	60.26 (+8.25)
8	✓	✓	✓	✓	✓	61.48 (+9.47)

proposed key modules (Exp. ID 8).

2) *Ablation Study on Quad-Directional Mixing*: We evaluate the effects of QuadMix paths through quantitative experiments and detailed feature visualization.

The effectiveness of quad-directional mixing paths. In this paper, we propose four comprehensive mixing paths designed for sufficient domain gap bridging. It naturally prompts us to explore the outcomes when only the intra/inter-mixed source or target domains are constructed or when templates are exclusively from the source or target domain. Table VI provides thorough ablation results for these scenarios. For fairness, we employ the flow-guided feature aggregation module (i.e., Exp. ID 6 in Table V) as the baseline (Exp. ID 0*).

It can be observed: (i) In Exp. ID 1, our $S \rightarrow T$ setting outperformed the CMOM [39] by 1.80% in mIoU, which also follows a source to target pasting paradigm. We attribute this improvement to the proposed flow-guided feature aggregation for domain alignment; (ii) The construction of intra/inter-mixed video domains always yields better results than solely one-way mixed domains. It is because the model can learn consistent spatio-temporal features with diverse domain contexts, with the feature-level mixing across two inter-mixed domains alleviating feature inconsistencies; (iii) Utilizing source domain templates commonly outperforms using target domain templates with higher predictive confidence. The overall mIOU exhibits further improvement when incorporating templates from both domains; (iv) More intriguingly, compared with incrementally combining various directional mixing as in Exp. ID 11, we not only reduce computational load significantly as shown in Table XI, but also achieve a mIoU gain of 0.92% to 61.48% by fully utilizing the enhanced quad-mixed domains for comprehensive domain bridging (Exp. ID 12).

It’s noteworthy that regardless of the intra/inter-mixing strategy adopted, the results of ablation studies in Table VI all surpass previous state-of-the-art methods CMOM [39] and TPL [38], which highlights the effectiveness of our QuadMix, a novel and unified perspective that has been largely overlooked by prior works [19], [21], [37], [39], [73], etc.

TABLE VI

ABLATION STUDIES OF THE QUAD-DIRECTIONAL MIXING PATHS ON SYNTHIA-SEQ \rightarrow CITYSCAPES-SEQ.

ID	$S \rightarrow T$	$T \rightarrow S$	$S \rightarrow S$	$T \rightarrow T$	$S \rightarrow (T \rightarrow T)$	$T \rightarrow (S \rightarrow S)$	mIOU (Gain)
CMOM	✓						56.31
0*							55.97
1	✓						58.11 (+2.14)
2			✓				57.84 (+1.87)
3	✓	✓					58.77 (+2.80)
4				✓			58.98 (+3.01)
5					✓		56.67 (+0.70)
6			✓	✓			59.24 (+3.27)
7	✓			✓			58.39 (+2.42)
8		✓	✓				59.55 (+3.58)
9	✓		✓				60.20 (+4.23)
10		✓		✓			59.39 (+3.42)
11	✓	✓	✓	✓			60.39 (+4.42)
12					✓	✓	61.48 (+5.51)

TABLE VII

ABLATION STUDIES ON CATEGORY SPACES FOR VIDEO PATCH TEMPLATE GENERATION ON SYNTHIA-SEQ \rightarrow CITYSCAPES-SEQ.

Mixed categories	Things	Stuffs	Movable	Stationary	All
mIOU(%)	58.53	57.50	58.29	55.55	61.48

Feature visualization for quad-directional mixing paths.

In Fig. 7, following experimental settings in Table VI, we present t-SNE [43] feature visualization for pure two domains (Exp. ID 0*), our **intra-mixed** domains (Exp. ID 6), one-way mixing (Exp. ID 1), two-way mixing (Exp. ID 3), and the proposed **QuadMix** (Exp. ID 12) from left to right. Notably, the number of points in Fig. 7(b)(d)(e) are equal. It can be found that quad-directional mixing effectively generalizes intra-domain features and enhances inter-domain features, addressing distinct point attributes within each domain. By sufficiently bridging domain gaps, it promotes dense knowledge transfer from the source domain to the target domain.

The effect of category selection on video patch template generation. The video patch templates used for quad-mixing involve patch regions corresponding to the randomly selected two categories from the source or target domain. We investigated the impact of category selection on generating video patch templates. Commonly, drawing on the concept from panoramic segmentation [82], objects are often categorized into “things” (e.g., *sign*, *car*) and “stuff” (e.g., *sky*, *road*). Therefore, in Table VII, we examined the results when the category selection comprised only “things” or “stuff”, as well as movable (e.g., *person*, *car*) or stationary (e.g., *sign*, *light*) objects. The experimental findings indicate that “things” and movable categories yield better results than “stuff” and stationary categories, and the model performs best when the category selection encompasses all categories. It highlights the versatility of our method across different categories.

3) *Ablation Study on Flow-Guided Feature Aggregation for Domain Alignment*: In this paper, to further address spatio-

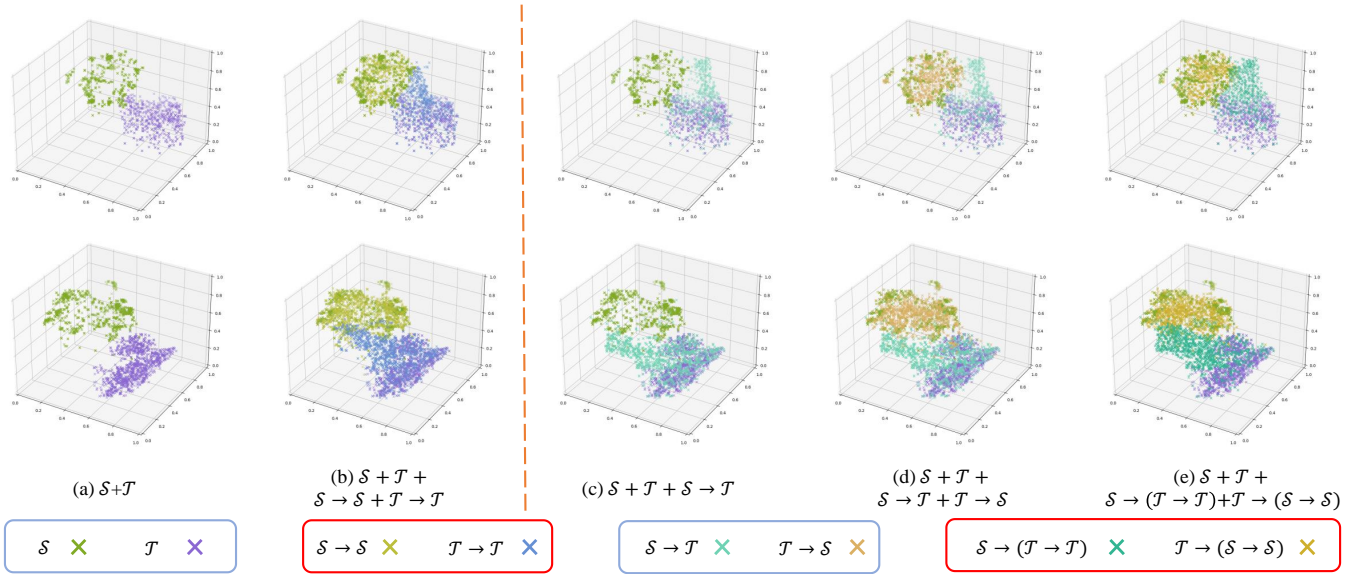


Fig. 7. T-SNE visualization of different mixing paradigms using *sign* (line one) and *pole* (line two) as examples. The experimental settings for subfigures (a) to (e) correspond to ablation studies Exp. ID 0*, ID 6, ID 1, ID 3, and ID 12 in Table VI. Note that the number of points in (b), (d), and (e) is consistent. Subfigure (b) shows intra-mixed domains with generalized feature embeddings, while (e) depicts quad-mixed domains with a more continuous and enhanced feature distribution, rather than a clustered one, which better addresses *distinct point attributes* of \mathcal{S} and \mathcal{T} for knowledge transfer. Please zoom in for details.

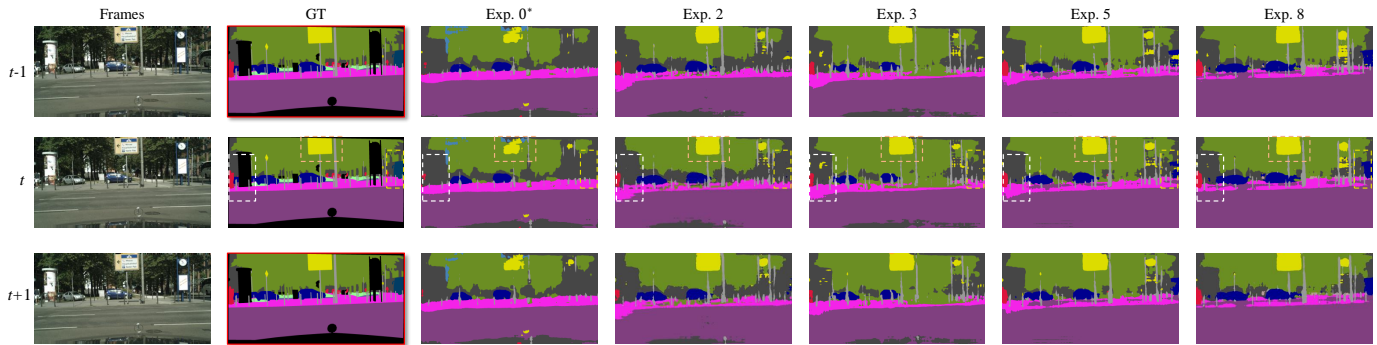


Fig. 8. Qualitative results of ablation studies in Table V for three consecutive frames on Synthia-Seq \rightarrow Cityscapes-Seq. The best results are obtained by integrating all of the proposed components (Exp. ID 8), especially for categories of *person*, *rider*, and *car*. Please zoom in for details.

TABLE VIII
ABLATION STUDIES ON FLOW-GUIDED FEATURE AGGREGATION FOR ALIGNMENT, AND IMAGE ENHANCEMENT \mathcal{A} ON THE TARGET DOMAIN.

Method	SYN-Seq \rightarrow City-Seq	VIPER \rightarrow Citys-Seq
w/o align	57.95	52.80
global align	58.24	53.62
flow-guided aggregation	61.48	56.16
w/o \mathcal{A}	60.23	55.25
w/ \mathcal{A}	61.48	56.16

temporal gaps within videos, we propose the optical guided video feature aggregation module for fine-grained alignment. When we exclusively substitute our fine-grained aggregation with treating video features as a whole [73], the mIOUs on two benchmarks decreased by 3.24% and 2.54%, respectively, as shown in Table VIII. It demonstrates the effectiveness of fine-grained aggregation in compressing video features into a more compact distribution, thereby reducing domain discrepancy

with fine-grained alignment. In addition, we also investigate the advantage of image enhancement \mathcal{A} in Eq. (22) and Eq. (24) for the target domain. Note that our contribution focuses on enhancing temporal coherence for domain alignment, which alignment loss is optimal to minimize discrepancies in aggregated features across domains is another research branch and goes beyond the main consideration of this work.

D. Further Analysis

In this section, we conduct further analysis using UDA-VSS benchmarks with the Deeplabv2 backbone by default.

1) *Hyperparameter Sensitivity*: For model optimization, we utilize two hyperparameters, $\lambda_{\mathcal{T}}$ in Eq. (22) and Eq. (24) and λ_f in Eq. (23). In Table IX, we progressively increase the values of $\lambda_{\mathcal{T}}$ and λ_f using Viper \rightarrow Cityscapes-Seq as an example to explore the hyperparameter sensitivity. The model achieves an mIOU of 56.16% when these parameters are set to 0.20 and 0.01 and a suboptimal mIOU of 55.20% when the two parameters are set to 1.00 and 0.10. The results display

TABLE IX
LOSS WEIGHTS SENSITIVITY ANALYSIS ON VIPER → CITYSCAPES-SEQ.

Weights	mIoU(%)
$\lambda_{\mathcal{T}}, \lambda_f = 0.10, 0.01$	54.56
$\lambda_{\mathcal{T}}, \lambda_f = 0.20, 0.01$	56.16
$\lambda_{\mathcal{T}}, \lambda_f = 0.50, 0.01$	54.49
$\lambda_{\mathcal{T}}, \lambda_f = 0.50, 0.10$	54.56
$\lambda_{\mathcal{T}}, \lambda_f = 0.70, 0.10$	54.58
$\lambda_{\mathcal{T}}, \lambda_f = 1.00, 0.10$	<u>55.20</u>

TABLE X
EFFECTIVENESS COMPARISON ON MODEL INITIALIZATION. THE “ORIGINAL” COLUMN DENOTES THE RESULTS OF ORIGINAL WORKS, WHILE THE “QUADMIX” COLUMN MEANS THE RESULTS OF OUR MODELS INITIALIZED WITH WARM-UP MODELS FROM THE “ORIGINAL” COLUMN.

Method	SYN-Seq → City-Seq		VIPER → Citys-Seq	
	Original	QuadMix	Original	QuadMix
ResNet-101 [80]	32.01	59.62	24.60	54.94
DA-VSN [6]	49.53	59.07	47.84	55.31
CMOM [39]	56.31	60.33	53.81	56.10
TPS [37]	53.76	61.48	48.91	56.16

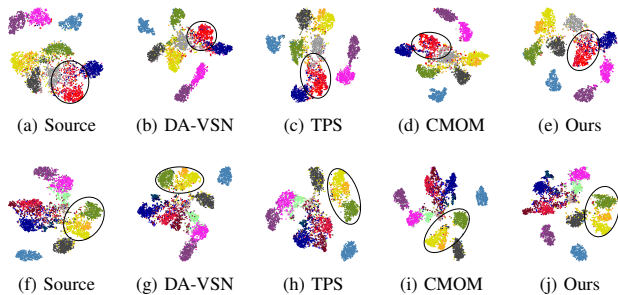


Fig. 9. T-SNE analysis of existing methods and our method on Synthia-Seq → Cityscapes-Seq (line one) and VIPER → Cityscapes-Seq (line two). Our model excels in learning more discriminative features of target videos within embedding space. Please zoom in for details.

slight fluctuations with parameter setting changes, showing our method’s robustness. For convenience, we set $\lambda_{\mathcal{T}}$ and λ_f to 1 for another Synthia-Seq → Cityscapes-Seq benchmark.

2) *Results with Model Initialization:* As shown in Table X, we achieve 59.62% and 54.94% mIoU on two benchmarks by end-to-end training, surpassing previous methods trained both end-to-end and in stages. Initializing our models with warm-up parameters from previous works in the “Original” column can further enhance adaptation. Notably, CMOM [39] initializes model parameters and generates initial pseudo-labels offline using a warm-up model trained in [6]. In contrast, we solely undergo model initialization. The above analysis underscores the remarkable adaptation of our method on UDA-VSS.

3) *The Throughput Measured for Different Modules:* In Table XI, we present the training time and GPU memory footprint associated with the integration of different components. “Src.” refers to training only with the source domain data. “QuadMix” corresponds to the ablation setting ID 11

TABLE XI
THROUGHPUT IS MEASURED WITH A BATCH SIZE OF 1. RESULTS ARE OBTAINED USING A V100-32G GPU. “QUADMIX” CORRESPONDS TO THE ABLATION SETTING ID 11 IN TABLE VI.

Modules	SYN-Seq → City-Seq		VIPER → City-Seq	
	Time (s/iter)	GPU memory	Time (s/iter)	GPU memory
Src.	1.40	8.78 G	1.38	8.78 G
SSL	2.31	12.52 G	2.34	13.54 G
QuadMix	3.78	21.24 G	3.99	21.90 G
QuadMix ⁻	4.26	24.92 G	4.37	25.90 G
Agg.	5.64	29.11 G	5.89	29.85 G

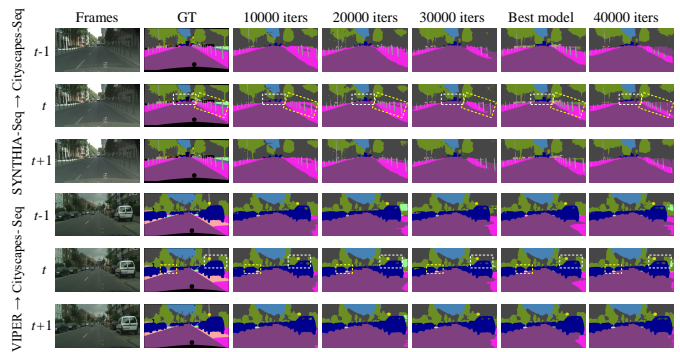


Fig. 10. Qualitative semantic segmentation results of our models at different training iterations for two UDA-VSS benchmarks. Please zoom in for details.

in Table VI. Compared to self-supervised learning “SSL”, the integration with QuadMix ($\mathcal{T} \rightarrow (\mathcal{S} \rightarrow \mathcal{S})$) and ($\mathcal{S} \rightarrow (\mathcal{T} \rightarrow \mathcal{T})$) leads to a modest increase in training time and GPU memory, and “Agg” exhibits relatively lighter overhead.

We also investigate the computational cost of Exp. ID 11 in Table VI (incrementally using $\mathcal{S} \rightarrow \mathcal{S} + \mathcal{T} \rightarrow \mathcal{T} + \mathcal{S} \rightarrow \mathcal{T} + \mathcal{T} \rightarrow \mathcal{S}$), which is higher in cost than our QuadMix. Notably, only adjacent frames and optical flow are required as inputs during model testing. In line with [6], [37]–[39], our method maintains similar inference speed and memory footprint.

4) *T-SNE Analysis on Two Benchmarks:* For better visualization, we present t-SNE [43] visualizations of video feature embeddings from three recent works and the source-only model, compared with our QuadMix in Fig.9. The dot colors for categories are consistent with Fig.6. We observe that category-wise clusters in recent methods tend to be more scattered and overlapped, whereas our method generates more compact clusters. For instance, in our method, categories like *perdon*, *rider*, and *fence* in Synthia-Seq → Cityscapes-Seq, and categories like *light*, *sign*, and *vegetation* in VIPER → Cityscapes-Seq, exhibit more compact intra-category distribution and more distinct inter-category differences, revealing better discriminative capability for the target domain.

5) *Results of Different Training Iterations:* In Fig. 10, we provide a more comprehensive presentation of semantic segmentation results of our models trained at different iterations. Notably, the best models for both two benchmarks emerge between the 35k and 40k iterations, providing a clearer insight into the evolution and stability of the training process.

V. CONCLUSION

This paper tackles the more challenging task of unified UDA-SS, addressing both video and image scenarios in a unified manner. Further, we propose QuadMix to address fragmentary and insufficient feature gap bridging caused by distinct point attributes. Specifically, we propose quad-directional intra- and inter-domain mixing at both pixel and feature levels, aiming to generalize intra-domain, enhance inter-domain, and alleviate feature inconsistencies. Additionally, we propose flow-guided video feature aggregation for fine-grained domain alignment, applicable to image scenarios as well. Extensive experiments on four benchmarks demonstrate our method's superiority across video and image scenarios. One limitation is that while quad-mixed samples enhance model adaptation, some unrealistic samples may mislead the model. Future work will explore generation-based reliable mixing for open-vocabulary domain adaptation using vision-language models.

ACKNOWLEDGMENT

This work is supported in part by the Major Program of the National Natural Science Foundation of China (NSFC) under Grants 61991400, and 61991404, in part by the NSFC under Grants 62103092, and Program of China Scholarship Council 202306080142. The authors appreciate Chunhua Shen and Lan Deng's helpful suggestions.

REFERENCES

- [1] K. Muhammad, T. Hussain, H. Ullah, J. Del Ser, M. Rezaei, N. Kumar, M. Hijji, P. Bellavista, and V. H. C. de Albuquerque, "Vision-based semantic segmentation in scene understanding for autonomous driving: Recent achievements, challenges, and outlooks," *IEEE Trans. Intell. Transp. Syst.*, vol. 23, no. 12, pp. 22 694–22 715, 2022.
- [2] Mo, Yujian, Wu, Yan, Yang, Xinneng, Liu, Feilin, and Liao, Yujun, "Review the state-of-the-art technologies of semantic segmentation based on deep learning," *Neurocomputing*, vol. 493, pp. 626–646, 2022.
- [3] Y. Jin, Y. Yu, C. Chen, Z. Zhao, P.-A. Heng, and D. Stoyanov, "Exploring intra- and inter-video relation for surgical semantic scene segmentation," *IEEE Trans. Med. Imaging*, vol. 41, no. 11, pp. 2991–3002, 2022.
- [4] N. Ghamsarian, M. Taschwer, R. Sznitman, and K. Schoeffmann, "Deep-pyramid: Enabling pyramid view and deformable pyramid reception for semantic segmentation in cataract surgery videos," in *Proc. Med. Image Comput. Comput. Assist. Intervent.* Springer, 2022, pp. 276–286.
- [5] N. Araslanov and S. Roth, "Self-supervised augmentation consistency for adapting semantic segmentation," in *Proc. IEEE Conf. Comput. Vis. Pattern Recognit.*, 2021, pp. 15 384–15 394.
- [6] D. Guan, J. Huang, A. Xiao, and S. Lu, "Domain adaptive video segmentation via temporal consistency regularization," in *Proc. IEEE Int. Conf. Comput. Vis.*, 2021, pp. 8053–8064.
- [7] M. Cordts, M. Omran, S. Ramos, T. Rehfeld, M. Enzweiler, R. Benenson, U. Franke, S. Roth, and B. Schiele, "The cityscapes dataset for semantic urban scene understanding," in *Proc. IEEE Conf. Comput. Vis. Pattern Recognit.*, 2016, pp. 3213–3223.
- [8] G. Ros, L. Sellart, J. Materzynska, D. Vazquez, and A. M. Lopez, "The synthia dataset: A large collection of synthetic images for semantic segmentation of urban scenes," in *Proc. IEEE Conf. Comput. Vis. Pattern Recognit.*, 2016, pp. 3234–3243.
- [9] S. R. Richter, Z. Hayder, and V. Koltun, "Playing for benchmarks," in *Proc. IEEE Int. Conf. Comput. Vis.*, 2017, pp. 2213–2222.
- [10] S. R. Richter, V. Vineet, S. Roth, and V. Koltun, "Playing for data: Ground truth from computer games," in *Proc. Eur. Conf. Comput. Vis.* Springer, 2016, pp. 102–118.
- [11] T. Vu, H. Jain, M. Bucher, M. Cord, and P. Pérez, "Advent: Adversarial entropy minimization for domain adaptation in semantic segmentation," in *Proc. IEEE Conf. Comput. Vis. Pattern Recognit.*, 2019, pp. 2517–2526.
- [12] Y. Zou, Z. Yu, B. Kumar, and J. Wang, "Unsupervised domain adaptation for semantic segmentation via class-balanced self-training," in *Proc. Eur. Conf. Comput. Vis.*, 2018, pp. 289–305.
- [13] F. Pan, I. Shin, F. Rameau, S. Lee, and I. S. Kweon, "Unsupervised intra-domain adaptation for semantic segmentation through self-supervision," in *Proc. IEEE Conf. Comput. Vis. Pattern Recognit.*, 2020, pp. 3764–3773.
- [14] Y. Zou, Z. Yu, X. Liu, B. Kumar, and J. Wang, "Confidence regularized self-training," in *Proc. IEEE Int. Conf. Comput. Vis.*, 2019, pp. 5982–5991.
- [15] D. Guan, J. Huang, S. Lu, and A. Xiao, "Scale variance minimization for unsupervised domain adaptation in image segmentation," *Pattern Recognit.*, vol. 112, p. 107764, 2021.
- [16] J. Huang, S. Lu, D. Guan, and X. Zhang, "Contextual-relation consistent domain adaptation for semantic segmentation," in *Proc. Eur. Conf. Comput. Vis.*, 2020, pp. 705–722.
- [17] J. Huang, D. Guan, A. Xiao, and S. Lu, "Rda: Robust domain adaptation via fourier adversarial attacking," in *Proc. IEEE Int. Conf. Comput. Vis.*, 2021, pp. 8988–8999.
- [18] Y. Yang and S. Soatto, "Fda: Fourier domain adaptation for semantic segmentation," in *Proc. IEEE Conf. Comput. Vis. Pattern Recognit.*, 2020, pp. 4085–4095.
- [19] W. Tranheden, V. Olsson, J. Pinto, and L. Svensson, "Dacs: Domain adaptation via cross-domain mixed sampling," in *Proc. IEEE Winter Conf. Appl. Comput. Vis.*, 2021, pp. 1379–1389.
- [20] L. Melas-Kyriazi and A. K. Manrai, "Pixmatch: Unsupervised domain adaptation via pixelwise consistency training," in *Proc. IEEE Conf. Comput. Vis. Pattern Recognit.*, 2021, pp. 12 435–12 445.
- [21] D. Kim, M. Seo, K. Park, I. Shin, S. Woo, I. S. Kweon, and D.-G. Choi, "Bidirectional domain mixup for domain adaptive semantic segmentation," in *Proc. AAAI Conf. Artif. Intell.*, vol. 37, no. 1, 2023, pp. 1114–1123.
- [22] Y. Cheng, F. Wei, J. Bao, D. Chen, and W. Zhang, "Adpl: Adaptive dual path learning for domain adaptation of semantic segmentation," *IEEE Trans. Pattern Anal. Mach. Intell.*, vol. 45, no. 8, pp. 9339–9356, 2023.
- [23] B. Xie, S. Li, M. Li, C. H. Liu, G. Huang, and G. Wang, "Sepico: Semantic-guided pixel contrast for domain adaptive semantic segmentation," *IEEE Trans. Pattern Anal. Mach. Intell.*, vol. 45, no. 7, pp. 9004–9021, 2023.
- [24] L. Hoyer, D. Dai, and L. Van Gool, "Daformer: Improving network architectures and training strategies for domain-adaptive semantic segmentation," in *Proc. IEEE Conf. Comput. Vis. Pattern Recognit.*, 2022, pp. 9924–9935.
- [25] J. Hoffman, E. Tzeng, T. Park, J.-Y. Zhu, P. Isola, K. Saenko, A. Efros, and T. Darrell, "Cycada: Cycle-consistent adversarial domain adaptation," in *Proc. Int. Conf. Mach. Learn.*, 2018, pp. 1989–1998.
- [26] Y. Zhang, H. Tang, K. Jia, and M. Tan, "Domain-symmetric networks for adversarial domain adaptation," in *Proc. IEEE Conf. Comput. Vis. Pattern Recognit.*, 2019, pp. 5031–5040.
- [27] M. Long, Z. Cao, J. Wang, and M. I. Jordan, "Conditional adversarial domain adaptation," in *Proc. Adv. Neural Inf. Process. Syst.*, 2018, pp. 1647–1657.
- [28] Y. Zhang, T. Liu, M. Long, and M. Jordan, "Bridging theory and algorithm for domain adaptation," in *Proc. Int. Conf. Mach. Learn.*, 2019, pp. 7404–7413.
- [29] A. Gretton, K. M. Borgwardt, M. J. Rasch, B. Schölkopf, and A. Smola, "A kernel two-sample test," *J. Mach. Learn. Res.*, vol. 13, no. 1, pp. 723–773, 2012.
- [30] B. Sun and K. Saenko, "Deep coral: Correlation alignment for deep domain adaptation," in *Proc. Eur. Conf. Comput. Vis.*, 2016, pp. 443–450.
- [31] K. Mei, C. Zhu, J. Zou, and S. Zhang, "Instance adaptive self-training for unsupervised domain adaptation," in *Proc. Eur. Conf. Comput. Vis.* Springer, 2020, pp. 415–430.
- [32] P. Zhang, B. Zhang, T. Zhang, D. Chen, Y. Wang, and F. Wen, "Prototypical pseudo label denoising and target structure learning for domain adaptive semantic segmentation," in *Proc. IEEE Conf. Comput. Vis. Pattern Recognit.*, 2021, pp. 12 414–12 424.
- [33] J. Li, K. Zhou, S. Qian, W. Li, L. Duan, and S. Gao, "Feature representation and reliable pseudo label retraining for cross-domain semantic segmentation," *IEEE Trans. Pattern Anal. Mach. Intell.*, pp. 1–13, 2022.
- [34] H. Tang, X. Zhu, K. Chen, K. Jia, and C. P. Chen, "Towards uncovering the intrinsic data structures for unsupervised domain adaptation using structurally regularized deep clustering," *IEEE Trans. Pattern Anal. Mach. Intell.*, vol. 44, no. 10, pp. 6517–6533, 2021.

- [35] I. Shin, K. Park, S. Woo, and I. S. Kweon, "Unsupervised domain adaptation for video semantic segmentation," *arXiv preprint arXiv:2107.11052*, 2021.
- [36] F. Pan, X. Yin, S. Lee, A. Niu, S. Yoon, and I. S. Kweon, "Moda: Leveraging motion priors from videos for advancing unsupervised domain adaptation in semantic segmentation," in *Proc. IEEE Conf. Comput. Vis. Pattern Recognit.*, 2024, pp. 2649–2658.
- [37] Y. Xing, D. Guan, J. Huang, and S. Lu, "Domain adaptive video segmentation via temporal pseudo supervision," in *Proc. Eur. Conf. Comput. Vis.*, 2022, pp. 621–639.
- [38] Y. Gao, Z. Wang, J. Zhuang, Y. Zhang, and J. Li, "Exploit domain-robust optical flow in domain adaptive video semantic segmentation," in *Proc. AAAI Conf. Artif. Intell.*, 2023, pp. 641–649.
- [39] K. Cho, S. Lee, H. Seong, and E. Kim, "Domain adaptive video semantic segmentation via cross-domain moving object mixing," in *Proc. IEEE Winter Conf. Appl. Comput. Vis.*, 2023, pp. 489–498.
- [40] R. Gopalan, R. Li, and R. Chellappa, "Unsupervised adaptation across domain shifts by generating intermediate data representations," *IEEE Trans. Pattern Anal. Mach. Intell.*, vol. 36, no. 11, pp. 2288–2302, 2013.
- [41] V. Olsson, W. Tranheden, J. Pinto, and L. Svensson, "Classmix: Segmentation-based data augmentation for semi-supervised learning," in *Proc. IEEE Winter Conf. Appl. Comput. Vis.*, 2021, pp. 1369–1378.
- [42] S. Yun, D. Han, S. J. Oh, S. Chun, J. Choe, and Y. Yoo, "Cutmix: Regularization strategy to train strong classifiers with localizable features," in *Proc. IEEE Int. Conf. Comput. Vis.*, 2019, pp. 6023–6032.
- [43] L. Van der Maaten and G. Hinton, "Visualizing data using t-sne," *J. Mach. Learn. Res.*, vol. 9, no. 11, pp. 2579–2605, 2008.
- [44] M. Xu, J. Zhang, B. Ni, T. Li, C. Wang, Q. Tian, and W. Zhang, "Adversarial domain adaptation with domain mixup," in *Proc. AAAI Conf. Artif. Intell.*, 2020, pp. 6502–6509.
- [45] G. Kim and S. Y. Chun, "Datid-3d: Diversity-preserved domain adaptation using text-to-image diffusion for 3d generative model," in *Proc. IEEE Conf. Comput. Vis. Pattern Recognit.*, June 2023, pp. 14203–14213.
- [46] J. Shen, Y. Qu, W. Zhang, and Y. Yu, "Wasserstein distance guided representation learning for domain adaptation," in *Proc. AAAI Conf. Artif. Intell.*, 2018, pp. 10285–10295.
- [47] Q. Zhang, J. Zhang, W. Liu, and D. Tao, "Category anchor-guided unsupervised domain adaptation for semantic segmentation," in *Proc. Adv. Neural Inf. Process. Syst.*, 2019, pp. 433–443.
- [48] Z. Wang, M. Yu, Y. Wei, R. Feris, J. Xiong, W.-m. Hwu, T. S. Huang, and H. Shi, "Differential treatment for stuff and things: A simple unsupervised domain adaptation method for semantic segmentation," in *Proc. IEEE Conf. Comput. Vis. Pattern Recognit.*, 2020, pp. 12635–12644.
- [49] J. Li, Z. Wang, Y. Gao, and X. Hu, "Exploring high-quality target domain information for unsupervised domain adaptive semantic segmentation," in *Proc. ACM Int. Conf. Multimed.*, 2022, pp. 5237–5245.
- [50] Y. Tsai, W. Hung, S. Schuster, K. Sohn, M. Yang, and M. Chandraker, "Learning to adapt structured output space for semantic segmentation," in *Proc. IEEE Conf. Comput. Vis. Pattern Recognit.*, 2018, pp. 7472–7481.
- [51] K. Mei, C. Zhu, J. Zou, and S. Zhang, "Instance adaptive self-training for unsupervised domain adaptation," in *Proc. Eur. Conf. Comput. Vis.*, 2020, pp. 415–430.
- [52] N. Karim, N. C. Mithun, A. Rajvanshi, H. Chiu, S. Samarasekera, and N. Rahnavard, "C-sfda: A curriculum learning aided self-training framework for efficient source free domain adaptation," in *Proc. IEEE Conf. Comput. Vis. Pattern Recognit.*, 2023, pp. 24120–24131.
- [53] X. Li, P. Ye, J. Li, Z. Liu, L. Cao, and F. Wang, "From features engineering to scenarios engineering for trustworthy ai: I&i, c&c, and v&v," *IEEE Intell. Syst.*, vol. 37, no. 4, pp. 18–26, 2022.
- [54] Y.-H. Tsai, W.-C. Hung, S. Schuster, K. Sohn, M.-H. Yang, and M. Chandraker, "Learning to adapt structured output space for semantic segmentation," in *Proc. IEEE Conf. Comput. Vis. Pattern Recognit.*, 2018, pp. 7472–7481.
- [55] S. K. Panda, Y. Lee, and M. K. Jawed, "Agronav: Autonomous navigation framework for agricultural robots and vehicles using semantic segmentation and semantic line detection," in *Proc. IEEE Conf. Comput. Vis. Pattern Recognit.*, 2023, pp. 6271–6280.
- [56] I. Alonso, L. Riazuelo, and A. C. Murillo, "Mininet: An efficient semantic segmentation convnet for real-time robotic applications," *IEEE Trans. Robot.*, vol. 36, no. 4, pp. 1340–1347, 2020.
- [57] S. Jain, X. Wang, and J. E. Gonzalez, "Accel: A corrective fusion network for efficient semantic segmentation on video," in *Proc. IEEE Conf. Comput. Vis. Pattern Recognit.*, 2019, pp. 8866–8875.
- [58] A. Ganesan, A. Vallet, Y. Kudo, S.-i. Maeda, T. Kerola, R. Ambrus, D. Park, and A. Gaidon, "Warp-refine propagation: Semi-supervised auto-labeling via cycle-consistency," in *Proc. IEEE Int. Conf. Comput. Vis.*, 2021, pp. 15499–15509.
- [59] Y. Zhang, S. Borse, H. Cai, and F. Porikli, "Auxadapt: Stable and efficient test-time adaptation for temporally consistent video semantic segmentation," in *Proc. IEEE Winter Conf. Appl. Comput. Vis.*, 2022, pp. 2339–2348.
- [60] F. Yuan, L. Zhang, X. Xia, Q. Huang, and X. Li, "A gated recurrent network with dual classification assistance for smoke semantic segmentation," *IEEE Trans. Image Process.*, vol. 30, pp. 4409–4422, 2021.
- [61] G. Sun, Y. Liu, H. Ding, T. Probst, and L. Van Gool, "Coarse-to-fine feature mining for video semantic segmentation," in *Proc. IEEE Conf. Comput. Vis. Pattern Recognit.*, 2022, pp. 3126–3137.
- [62] P. Hu, F. Caba, O. Wang, Z. Lin, S. Sclaroff, and F. Perazzi, "Temporally distributed networks for fast video semantic segmentation," in *Proc. IEEE Conf. Comput. Vis. Pattern Recognit.*, 2020, pp. 8818–8827.
- [63] M. Guo, T. Xu, J. Liu, Z. Liu, P. Jiang, T. Mu, S. Zhang, R. R. Martin, M. Cheng, and S. Hu, "Attention mechanisms in computer vision: A survey," *Comput. Vis. Media*, vol. 8, no. 3, pp. 331–368, 2022.
- [64] J. Lao, W. Hong, X. Guo, Y. Zhang, J. Wang, J. Chen, and W. Chu, "Simultaneously short-and long-term temporal modeling for semi-supervised video semantic segmentation," in *Proc. IEEE Conf. Comput. Vis. Pattern Recognit.*, 2023, pp. 14763–14772.
- [65] J. Zhuang, Z. Wang, and Y. Gao, "Semi-supervised video semantic segmentation with inter-frame feature reconstruction," in *Proc. IEEE Conf. Comput. Vis. Pattern Recognit.*, 2022, pp. 3263–3271.
- [66] X. Song, S. Zhao, J. Yang, H. Yue, P. Xu, R. Hu, and H. Chai, "Spatio-temporal contrastive domain adaptation for action recognition," in *Proc. IEEE Conf. Comput. Vis. Pattern Recognit.*, 2021, pp. 9787–9795.
- [67] H. Coskun, M. Z. Zia, B. Tekin, F. Bogo, N. Navab, F. Tombari, and H. Sawhney, "Domain-specific priors and meta learning for few-shot first-person action recognition," *IEEE Trans. Pattern Anal. Mach. Intell.*, vol. 45, no. 6, pp. 6659–6673, 2023.
- [68] D. Niu, A. Bar, R. Herzig, T. Darrell, and A. Rohrbach, "Object-based (yet class-agnostic) video domain adaptation," *arXiv preprint arXiv:2311.17942*, 2023.
- [69] Y. Xu, H. Cao, K. Mao, Z. Chen, L. Xie, and J. Yang, "Aligning correlation information for domain adaptation in action recognition," *IEEE Trans. Neural Netw. Learn. Syst.*, pp. 1–12, 2022.
- [70] A. Radford, L. Metz, and S. Chintala, "Unsupervised representation learning with deep convolutional generative adversarial networks," in *Proc. Int. Conf. Learn. Representations*, 2016, pp. 1–16.
- [71] X. Wu, Z. Wu, J. Wan, L. Ju, and S. Wang, "Is it necessary to transfer temporal knowledge for domain adaptive video semantic segmentation?" in *Proc. Eur. Conf. Comput. Vis.*, 2022, pp. 357–373.
- [72] A. Tarvainen and H. Valpola, "Mean teachers are better role models: Weight-averaged consistency targets improve semi-supervised deep learning results," in *Proc. Adv. Neural Inf. Process. Syst.*, 2017, pp. 1195–1204.
- [73] L. Gao, J. Zhang, L. Zhang, and D. Tao, "Dsp: Dual soft-paste for unsupervised domain adaptive semantic segmentation," in *Proc. ACM Int. Conf. Multimed.*, 2021, pp. 2825–2833.
- [74] J. Moon, J. Kim, Y. Shin, and S. Hwang, "Confidence-aware learning for deep neural networks," in *Proc. Int. Conf. Mach. Learn.* PMLR, 2020, pp. 7034–7044.
- [75] H. Mai, R. Sun, Y. Wang, T. Zhang, and F. Wu, "Pay attention to target: Relation-aware temporal consistency for domain adaptive video semantic segmentation," in *Proc. AAAI Conf. Artif. Intell.*, vol. 38, no. 5, 2024, pp. 4162–4170.
- [76] H. Ma, X. Lin, and Y. Yu, "I2f: A unified image-to-feature approach for domain adaptive semantic segmentation," *IEEE Trans. Pattern Anal. Mach. Intell.*, vol. 46, no. 3, pp. 1695–1710, 2024.
- [77] T.-D. Truong, N. Le, B. Raj, J. Cothren, and K. Luu, "Freedom: Fairness domain adaptation approach to semantic scene understanding," in *Proc. IEEE Conf. Comput. Vis. Pattern Recognit.*, 2023, pp. 19988–19997.
- [78] L. Chen, G. Papandreou, I. Kokkinos, K. Murphy, and A. L. Yuille, "DeepLab: Semantic image segmentation with deep convolutional nets, atrous convolution, and fully connected crfs," *IEEE Trans. Pattern Anal. Mach. Intell.*, vol. 40, no. 4, pp. 834–848, 2017.
- [79] A. Dosovitskiy, P. Fischer, E. Ilg, P. Hausser, C. Hazirbas, V. Golkov, P. Van Der Smagt, D. Cremers, and T. Brox, "Flownet: Learning optical flow with convolutional networks," in *Proc. IEEE Int. Conf. Comput. Vis.*, 2015, pp. 2758–2766.
- [80] K. He, X. Zhang, S. Ren, and J. Sun, "Deep residual learning for image recognition," in *Proc. IEEE Conf. Comput. Vis. Pattern Recognit.*, 2016, pp. 770–778.

- [81] J. Deng, W. Dong, R. Socher, L. Li, K. Li, and L. Feifei, "Imagenet: A large-scale hierarchical image database," in *Proc. IEEE Conf. Comput. Vis. Pattern Recognit.*, 2009, pp. 248–255.
- [82] A. Kirillov, K. He, R. Girshick, C. Rother, and P. Dollar, "Panoptic segmentation," in *Proc. IEEE Conf. Comput. Vis. Pattern Recognit.*, 2019, pp. 9404–9413.



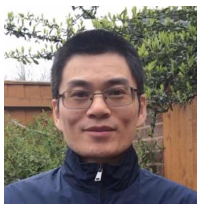
Zhe Zhang received the BS degree in the College of Information Science and Engineering, Northeastern University, China, in 2021. He is currently working toward a Ph.D. degree in the State Key Laboratory of Synthetical Automation for Process Industries, Northeastern University, Shenyang, China. His current research interests include computer vision, deep learning, video representation learning, multi-modal learning, and their applications in industrial fields.



Gaochang Wu received the BE and MS degrees in mechanical engineering in Northeastern University, Shenyang, China, in 2013 and 2015, respectively, and Ph.D. degree in control theory and control engineering in Northeastern University, Shenyang, China in 2020. He is currently an associate professor in the State Key Laboratory of Synthetical Automation for Process Industries, Northeastern University. His current research interests include image processing, light field processing, and deep learning.



Jing Zhang (Senior Member, IEEE) is currently a Research Fellow at the School of Computer Science, The University of Sydney. He has published more than 60 papers in prestigious conferences and journals, such as CVPR, ICCV, ECCV, NeurIPS, ICLR, IEEE TPAMI, and IJCV. His research interests include computer vision and deep learning. He is also a Senior Program Committee Member of the AAAI Conference on Artificial Intelligence and the International Joint Conference on Artificial Intelligence. He serves as a regular reviewer for many prestigious journals and conferences.



Xiatian Zhu received the PhD degree from the Queen Mary University of London. He is a senior lecturer with Surrey Institute for People-Centred Artificial Intelligence, and Centre for Vision, Speech and Signal Processing (CVSSP), University of Surrey, Guildford, U.K. He won the Sullivan Doctoral Thesis Prize 2016. He was a research scientist with Samsung AI Centre, Cambridge, U.K. His research interests include computer vision and machine learning.



Dacheng Tao (Fellow, IEEE) is currently a professor in computer science and an Australian laureate fellow with the Sydney AI Centre and the School of Computer Science, Faculty of Engineering, University of Sydney. He mainly applies statistics and mathematics to artificial intelligence and data science, and his research is detailed in one monograph and more than 200 publications in prestigious journals and proceedings at leading conferences. He received the 2015 and 2020 Australian Eureka Prize, the 2018 IEEE ICDM Research Contributions Award, and the 2021 IEEE Computer Society McCluskey Technical Achievement Award. He is a fellow of the Australian Academy of Science, AAAS, ACM, and IEEE.



Tianyou Chai (Life Fellow, IEEE) received the Ph.D. degree in control theory and engineering from Northeastern University, Shenyang, China, in 1985. He became a Professor at Northeastern University in 1988. He is the Founder and the Director of the Center of Automation, Northeastern University, which became the National Engineering and Technology Research Center and the State Key Laboratory. He was the Director of the Department of Information Science, National Natural Science Foundation of China, from 2010 to 2018. He has developed control technologies with applications to various industrial processes. He has published more than 320 peer-reviewed international journal articles. His current research interests include modeling, control, optimization, and integrated automation of complex industrial processes.

Dr. Chai is a member of the Chinese Academy of Engineering and a Fellow of International Federation for Automatic Control (IFAC). His paper titled "Hybrid intelligent control for optimal operation of shaft furnace roasting process" was selected as one of the three best papers for the Control Engineering Practice Paper Prize for the term 2011–2013. For his contributions, he has won five prestigious awards of the National Natural Science, the National Science and Technology Progress, and the National Technological Innovation, the 2007 Industry Award for Excellence in Transitional Control Research from IEEE Multi-Conference on Systems and Control, and the 2017 Wook Hyun Kwon Education Award from the Asian Control Association.